Enhancement of the thermoelectric properties in nanoscale and nanostructured materials

Jeannine R. Szczech, Jeremy M. Higgins and Song Jin*

Received 20th August 2010, Accepted 10th November 2010
DOI: 10.1039/c0jm02755c

Thermoelectric materials can be used for solid state power generation and heating/cooling applications. The figure of merit of thermoelectric materials, ZT, which determines their efficiency in a thermoelectric device, remains low for most conventional bulk materials. Nanoscale and nanostructured thermoelectric materials are promising for increasing ZT relative to the bulk. This review introduces the theory behind thermoelectric materials and details the predicted and demonstrated enhancements of ZT in nanoscale and nanostructured thermoelectric materials. We discuss thin films and superlattices, nanowires and nanotubes, and nanocomposites, providing a ZT comparison among various families of nanocomposite materials. We provide some perspectives regarding the origin of enhanced ZT in nanoscale and nanostructured materials and suggest some promising and fruitful research directions for achieving high ZT materials for practical applications.

1. Thermoelectricity: background and theory

The demand for energy is projected to grow by 44% from 2006 to 2030 as both world population and per capita energy consumption continue to increase.[1] Concern over the negative impact of increasing anthropogenic carbon load on global climate reveals the need for technologies that increase the net power output of our fuels and the exploration of technologies for renewable energy generation.

Energy generation and utilization efficiency can be improved by recovering waste heat from industrial processes or automobiles using the thermoelectric process known as the Seebeck effect.[2–5] The direct conversion of thermal energy to electrical energy that occurs when a temperature gradient is applied across a material is given by $\Delta V = S\Delta T$, where ΔV is the generated voltage, S is the Seebeck coefficient or thermopower, and ΔT is the magnitude of the temperature difference. The Seebeck voltage arises from the perturbation of the equilibrium distribution of charge carriers, described by the Fermi–Dirac distribution. When a temperature gradient is established, charge carriers diffuse from high temperature to low temperature regions to achieve a new equilibrium distribution. When two chemically dissimilar materials in a thermal gradient are connected, a circuit is formed in which the induced voltage drives the migration of charge carriers (*i.e.* a current) that can be used to perform useful work (Fig. 1a).

Degenerately doped semiconductors that have Seebeck voltages typically on the order of a few tens or hundreds of microvolts per degree are the most commonly-used materials in thermoelectric applications. Carrier diffusion dominates the Seebeck voltage in degenerate semiconductors; however, in samples with low carrier concentrations an enhanced thermoelectric voltage can arise from the significant phonon-electron scattering of the Seebeck voltage-induced drift current. This scattering, called phonon drag, decreases with increasing carrier concentration.[2] Radioisotope thermoelectric generators (RTGs) using the

Department of Chemistry, University of Wisconsin–Madison, 1101 University Avenue, Madison, Wisconsin, 53706, USA. E-mail: jin@chem.wisc.edu

Jeannine R. Szczech

Jeannine Szczech studied chemistry at the University of WI–Madison, graduating with a B.S. degree in 2005. She remained at the UW–Madison to continue her studies in the Song Jin research group, earning a Ph.D. in Materials Chemistry in 2010. Her research interests include nanoscale materials with applications in thermoelectric and electrochemical devices.

Jeremy M. Higgins

Jeremy Higgins received his B.S. from the University of Pittsburgh in 2005. He is currently a Ph.D. candidate at the University of Wisconsin–Madison working in the Song Jin research group. His thesis work focuses on synthesis of novel silicide nanowire materials and elucidation of the silicide nanowire growth mechanism with special emphasis on nanowires for use in thermoelectric and spintronic applications.

Seebeck effect have been used to power unmanned space flights, and thermoelectric power generators have been used in terrestrial applications to provide power in remote locations.[4]

The Peltier effect allows thermoelectricity to be utilized for solid state heating or cooling. In such applications, an electric current applied to a thermocouple causes heat to be emitted from or absorbed at the junction between the two materials (Fig. 1b), with the heat flow given as $Q = \Pi I$, where Q is the heat absorbed or emitted, Π is the Peltier coefficient, and I is the applied current. By changing the direction of the applied current, the operation of the junction can be switched from heating to cooling. The Seebeck and Peltier coefficients can be related to one another by the Kelvin relation, $\Pi = ST$. Consumer products using the Peltier effect, such as portable picnic coolers and temperature-controlled automobile seats, are becoming increasingly common. The Peltier effect has also been used to provide solid state cooling for scientific instruments. There is a third thermoelectric effect, the Thomson effect, but this will not be discussed in this review.[2,3]

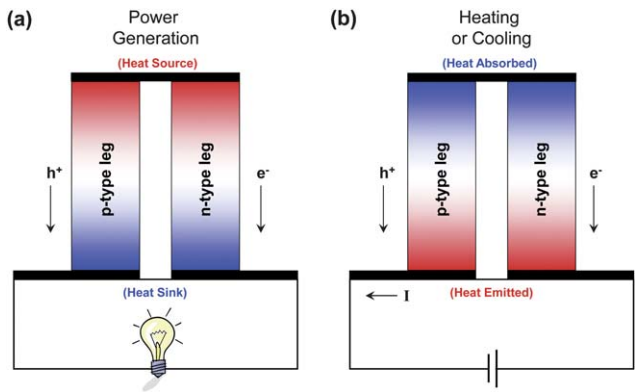

Fig. 1 Schematic drawing of thermoelectric devices used for (a) power generation and (b) heating and cooling applications.

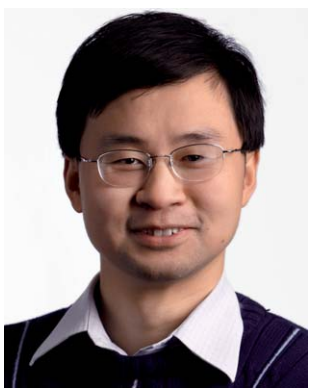

Song Jin

Song Jin received his B.S. from Peking University in 1997 and his Ph.D. from Cornell University in 2002. He has been at the University of Wisconsin–Madison since 2004 and is currently an associate professor of chemistry. He is interested in the chemistry and physics of nanomaterials. Dr. Jin studies the fundamental formation mechanisms of nanowires, their novel physical properties, and applications in renewable energy such photovoltaic and thermoelectric energy conversion, and energy storage. He has received the NSF Career Award and ACS Exxon Mobil Solid State Fellowship, is a Sloan Research Fellow and a Research Corporation Cottrell Scholar, and was recognized as a TR35 by MIT Technology Review magazine.

The efficiency of a thermoelectric material is described by its dimensionless figure of merit, ZT, which ties the material properties to its conversion efficiency. The figure of merit is defined as:

$$ZT = \frac{S^2\sigma T}{\kappa_{lattice} + \kappa_{electronic}} \quad (1)$$

where σ is the electrical conductivity, and κ_{lattice} and $\kappa_{\text{electronic}}$ are the lattice and electronic contributions to the thermal conductivity, respectively. The maximum power is proportional to $S^2\sigma$, referred to as the power factor. To maximize ZT, high thermopower, high electrical conductivity, and low thermal conductivity are required, but the interdependence of these material properties makes manipulation difficult. The Seebeck coefficient is most generally calculated using Fermi–Dirac statistics,[2] however, for a highly degenerate electron gas (*i.e.* metals and highly degenerate semiconductors) the Mott–Jones relation applied to simple transport models[6] (parabolic band model in the energy independent scattering approximation) is illustrative:

$$S = \frac{8\pi^2 k_B^2}{3eh^2} m^* T \left(\frac{\pi}{3n}\right)^{\frac{2}{3}} \quad (2)$$

where k_B is the Boltzmann constant, e is the carrier charge, h is Planck's constant, m^* is the effective mass of the charge carrier, and n is the carrier concentration. As an example, an increase in carrier concentration decreases the thermopower, but the electrical conductivity increases with the carrier concentration:

$$\sigma = ne\mu \quad (3)$$

where e is the carrier charge, and μ is the carrier mobility. This converse behavior constrains our ability to maximize the power factor through doping alone.[6] While universally accepted in metallic systems, the Wiedemann–Franz law can also be used to estimate the electronic contribution to the thermal conductivity for degenerate semiconductors, revealing that materials with high electrical conductivity also have high thermal conductivities:

$$\kappa_{electronic} = \sigma LT \quad (4)$$

where L is the Lorentz number, typically taken as 2.4×10^{-8} $J^2/K^2 \cdot C^2$ in materials having a highly degenerate electron gas. Therefore, efforts to improve ZT by increasing the electrical conductivity are potentially detrimental due to increases in the thermal conductivity. The interdependence of the thermopower, electrical conductivity, and thermal conductivity can be seen clearly in Fig. 2, which is calculated for Bi_2Te_3.[6]

The best bulk thermoelectric materials are typically degenerate semiconductors that have high carrier mobilities and a low electronic contribution to the thermal conductivity. Although metals have high electrical conductivity and exhibit the thermoelectric effect, their thermopowers are usually too low and thermal conductivity too high to generate sufficient power to be used in practical devices. Thermal conductivity in semiconductors is due primarily to lattice heat transport and can be approximated by:

$$\kappa_{lattice} = \frac{1}{3}\left(C_v \nu_s \lambda_{ph}\right) \quad (5)$$

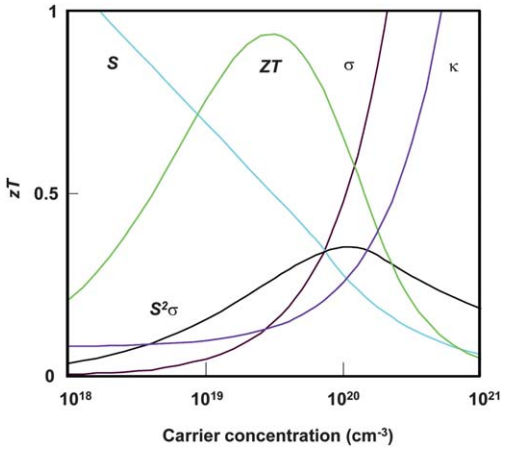

Fig. 2 Interdependence of the thermopower (S), electrical conductivity (σ), and thermal conductivity (κ). Reproduced from ref. 6, Nature Publishing Group.

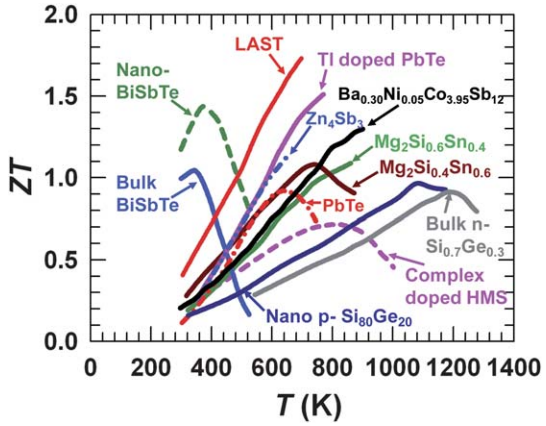

Fig. 3 State-of-the-art comparison of ZT in conventional bulk materials and nanostructured composite materials. Courtesy of Prof. Li Shi (University of Texas–Austin).

where C_v is the heat capacity (specific heat of the lattice), v_s is the sound velocity, and λ_{ph} is the phonon mean free path (mfp).[7] Semiconducting materials possessing low sound velocities and short phonon mfps will have favorably low thermal conductivities, making them good candidates for high ZT thermoelectric applications. While no theoretical limit for the maximum attainable ZT exists, research on thermoelectric materials, such as Bi_2Te_3, Sb_2Te_3, and $Si_{1-x}Ge_x$, during the last four decades has revealed a practical ceiling of $ZT \approx 1$ for simple crystalline bulk materials originating from the interdependence of the transport properties and thermopower.[8] For thermoelectrics to be competitive with current technologies, ZT must be enhanced to above 1.5 for power generation[4] and 2–4 for cooling[5,8] applications, respectively.

The ZT of conventional bulk materials remained near unity for many decades. However, in the last decade research in the discovery of new bulk materials with better thermoelectric performance and the development of nanoscale and nanostructured materials have independently achieved ZT above 1.5 with further increases anticipated. A state-of-the-art comparison of ZT in some conventional bulk thermoelectric materials and more recent nanoscale and nanostructured thermoelectric materials is shown in Fig. 3. The ZT enhancement in these nanomaterials has resulted primarily from decreased thermal conductivity,[9–16] although enhancements resulting from increased thermopower are also believed to be possible.[17–19]

This review seeks to provide a broad overview of the effect of nanoscale morphology on enhancement of the thermoelectric properties of nanostructured or nanoscale materials. We will critically discuss thin films and superlattices, nanowires and nanotubes, and nanocomposites, but will not attempt to provide an exhaustive review of all works in each of these areas. For a more detailed look at the enhancements for each of the different nanomorphologies, the reader is referred to recent reviews with more narrow focus on nanoscale (thin films, superlattices, and nanowires)[20] or bulk nanostructured[6,21–24] morphologies. Reviews highlighting the classical approaches to maximizing ZT are also available.[6,23,25] We first provide a description of the classical approaches used for achieving high ZT in bulk materials. A brief review of the theory underlying potential thermoelectric enhancements which may result from exploiting both quantum size and interface effects will then be presented, followed by a survey of the thermoelectric performance of materials with various nanoscale morphologies. Finally, we will conclude with a comparison of the families of nanocomposite materials.

2. Classical approaches to enhance bulk thermoelectric materials

The classical approaches to achieving high values of ZT rely on strategies aimed at either increasing the power factor or decreasing the thermal conductivity. These strategies include the use of materials composed of elements having large atomic masses; the design of alloys to create point defects that scatter heat carrying phonons; the use of materials with complex crystal structures or crystals containing constituents which do not have well-defined lattice positions; and the use of dopants with energy levels nearly resonant with a material's Fermi level. The theory behind each of these approaches will be briefly discussed here.

2.1 Heavy element compound semiconductors

Materials composed of heavy elements have low sound velocities and correspondingly low thermal conductivities. Many commonly used thermoelectric materials such as Bi_2Te_3, PbTe and BiSb can be classified as heavy element compound semiconductors. The thermal conductivities of these materials are quite low, typically ranging from 2–3 W/m·K for Bi_2Te_3 and 2–10 W/m·K for PbTe.[26] Conventionally, samples of these materials are either very pure single crystals or polycrystalline, but not nanocrystalline, samples prepared using various metallurgical methods.[2,27] Despite many decades of research into these thermoelectric materials, maximum ZT values remained near unity, perhaps suggesting a practical maximum ZT possible for simple binary and ternary compounds using this approach.

2.2 Alloy point defect scattering

To obtain high values of ZT, it is necessary to reduce the phonon mfp to be as close as possible to the minimum (amorphous) phonon mfp. This can be done through alloying, which creates point defects due to mass fluctuations in the crystal lattice.[28] Through judicious choice of the elements used in the alloy, for example by substituting host atoms with an element from the same group in the periodic table, carrier scattering at these defects can be minimized.[29] The quintessential example of an alloy-based thermoelectric material is $Si_{1-x}Ge_x$. Because elemental silicon and germanium have the same crystal structure, lattice order is preserved during alloying. However, charge carrier mobility is reduced in alloy crystals when the host and guest elements have moderately different electronegativities, due to the fluctuations in electric potential felt by charge carriers as they move through the crystal.[30] The electronegativity difference between silicon and germanium is large enough to generate electric potential fluctuations, which reduces the carrier mobility of $Si_{1-x}Ge_x$ alloys as germanium content increases.[31] Despite its effects on other important material parameters, such as the electrical conductivity, alloy point defect scattering can result in significantly decreased thermal conductivity giving rise to a net increase in ZT. For example, the thermal conductivity of undoped $Si_{1-x}Ge_x$ crystalline alloy was reported to decrease by an order of magnitude compared to undoped Si over a wide range of x.[32] This approach has been successfully used to produce the state-of-the-art thermoelectric materials used in commercial applications for many decades.[33]

2.3 Complex crystal structures

A more modern strategy in the search for high ZT thermoelectric materials is to seek out materials that have high electronic conductivity due to their highly periodic crystal structure but low thermal conductivity resulting from the complex structural features of the crystal lattice. This approach has been termed the phonon-glass electron-crystal (PGEC) approach.[30] The partially-filled clathrates[35] and skutterudites[36] are two heavily studied families of materials believed to be PGECs. These structures contain large voids which can be filled with loosely-bound atoms that 'rattle' within the structure, leading to decreased phonon lifetimes and the name of "rattler" compounds. ZTs near 1.35 have been reported for the skutterudite $Ba_rIn_sCo_4Sb_{12}$[34] and the clathrate $Ba_8Ga_{16}Ge_{13}$.[35]

Materials with complex crystal structures and large unit cell constants are also being pursued in hopes of discovering effective PGECs. Zintl compounds,[6,25] such as $Yb_{14}MnSb_{11}$ (Fig. 4a), are a promising example of such a system. They contain a valence-balanced combination of cations and covalently bonded anionic units. The combination of covalent and ionic bonding leads to higher charge mobilities than purely ionic compounds and large, complex unit cells with intrinsically low thermal conductivity. $Yb_{14}MnSb_{11}$ is an excellent material for high temperature thermoelectrics having reported ZT of 1.0 at 1223 K[36] and up to 1.3 with optimized alloying.[37] Nowotny chimney ladder[38–40] (NCL) compounds (Fig. 4b) are another class of complex crystal structure materials promising as PGECs. They have a variable-length, columnar sublattice of non-metal atoms (ladders) residing in the channels (chimneys) of a metal atom sublattice, forming homologous families of complex structures with variable unit cell length or incommensurate crystal structures. Such materials approach the borderline between crystalline solids and amorphous materials. While most NCL compounds are metallic, some have narrow bandgap ground states which in conjunction with their structure-derived low thermal conductivity results in respectable ZT.[38] For example, $MnSi_{1.7}$, also known as higher manganese silicides (HMS), has reported ZT up to 0.7–0.8 when appropriately doped.[38,40,41] The lattice contribution of the thermal conductivity is expected to be quite low in these promising thermoelectric materials, leading to high values of ZT.

2.4 Resonant energy level doping

Optimization of carrier concentration is always required to maximize ZT regardless of the thermoelectric material, as clearly shown in Fig. 2. When a dopant has energy levels near the Fermi level, ZT may be further enhanced by increasing the density of states (DOS) near the Fermi level and improving the thermopower. For example, $ZT = 1.5$ at 773 K was recently reported in Tl-doped PbTe,[42] a doubling of ZT compared to the state-of-the-art bulk PbTe (~ 0.7).[6] It is believed that the thermopower was enhanced by a distortion of the DOS near the Fermi level, resulting from resonant energy levels introduced by the Tl dopant. When a donor or acceptor level lies near the Fermi level (Fig. 5a), the local DOS is increased leading to a net increase in the carrier effective mass without a significant change in the carrier concentration. This increased effective mass should lead directly to an increase in thermopower, potentially overcoming the detrimental effects such doping is expected to have on carrier mobility. For the case of Tl-doped PbTe, the effective mass was observed to increase by a factor of 3, while the mobility was observed decrease by a factor between 3 and 5. The thermal conductivity was similar to bulk PbTe. The net effect was a significant increase in ZT (Fig. 5b) as compared to using a dopant which does not have a suitably located energy level.

2.5 The challenge of thermoelectric commercialization

A number of bulk thermoelectric materials with $ZT \approx 1$ have found limited commercial use in applications where the reliability, compact size, and low noise of a solid-state device is more important than efficiency, such as remote power generation and space exploration, and in niche applications, including electric picnic coolers, temperature-controlled automobile seats, and cooling devices for scientific instruments. However, the ZT of these materials must be improved to above 1.5 for waste heat recovery power generation[4] or up to 2–4 for cooling[5,8] and other applications (depending on the specific application), before they will become competitive with current widely-used technologies, such as power generation from the combustion of fossil fuels and Freon-based refrigeration.[4,5,8] In addition, thermoelectric materials also need to be inexpensive, robust, viable for integration into practical devices, and ideally use nontoxic and earth abundant materials, especially for large scale applications, such as automobile waste heat recovery.[5] This is a formidable challenge. Due to the aforementioned interdependence of materials properties, it is difficult to engineer bulk materials with high figures

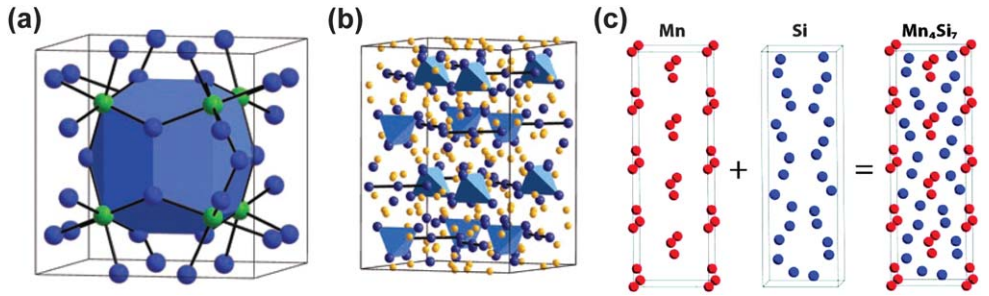

Fig. 4 (a) The crystal structure of the skutterudite compound $CoSb_3$, showing the formation of large void spaces (blue polygon) formed by the arrangement of tilted octahedra of Co (green) and Sb (dark blue). (b) The crystal structure of the Zintl compound $Yb_{14}MnSb_{11}$, consisting of $[Sb_3]^{7-}$ trimers (dark blue), $[MnSb_4]^{2-}$ tetrahedral (turquoise), isolated Sb atoms (dark blue), and the Yb^{2+} sublattice (yellow). Reproduced from ref. 6, Nature Publishing Group. (c) A model of Nowotny chimney ladder structures, using Mn_4Si_7 as an example, showing the formation of the complex crystal structure from Mn and Si sublattices. Reproduced from ref. 39, the American Chemical Society.

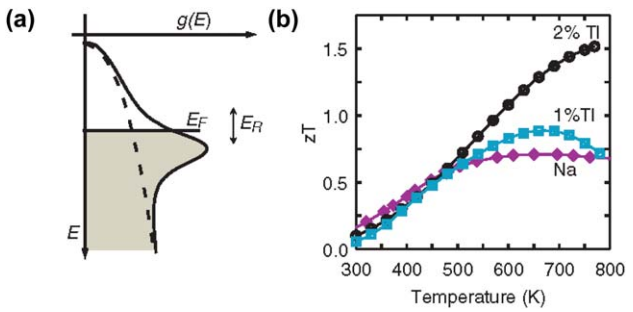

Fig. 5 (a) Schematic illustration of the density of states ($g(E)$) enhancement that can be achieved when the Fermi level (E_F) lies within the energy range E_R from the distortion caused by the resonant energy level. The dashed line corresponds to pure PbTe, and the solid line corresponds to Tl-PbTe (with resonant energy levels from Tl). (b) ZT corresponding to $Tl_{0.02}Pb_{0.98}Te$ (black circles), $Tl_{0.01}Pb_{0.99}Te$ (turquoise squares), and conventional Na-PbTe (purple diamonds). Reproduced from ref. 42, Science/AAAS Publications.

of merit. We therefore look to nanostructures to improve the overall efficiency of thermoelectric materials for their unique ability to tune material properties by reducing their size and dimensionality.

3. The nanoscale approach to enhancing thermoelectric performance

Reduced dimensionality has been considered for many years[43] as an approach to improve low cost bulk materials with poor thermoelectric properties, such as semimetallic bismuth,[44] metallic zinc,[45] and semiconducting silicon,[13,14,46] by decoupling the interdependence of S, σ, and κ. Promising demonstrations of these materials have renewed motivation for research into thermoelectric nanomaterials. Two distinct strategies for enhancing the thermoelectrics properties of a material using nanoscale or nanostructured morphologies are now being developed: (1) enhancement of the DOS near the Fermi level *via* quantum confinement to increase the thermopower, and (2) increasing the presence of interfaces and surfaces to enhance phonon scattering.

The quantum confinement approach seeks to increase the thermoelectric power factor through an increase of the electronic DOS near the Fermi level. This is accomplished by making the size scale of the material comparable to the spatial extent of the electronic wavefunction confining the electrons in one or more dimension. If electron scattering is assumed to be energy independent (*i.e.* $\mu(E) = \mu$), then the electrical conductivity is directly proportional to the DOS.[23] According to the Mott–Jones relation, which is only strictly valid in the case of metals and highly degenerate semiconductors, this would result in enhancement of the thermopower by increasing the slope of the DOS at the Fermi level:[47]

$$S = \frac{\pi^2}{3}\frac{k^2 T}{e}\left(\frac{\partial \log \sigma(E)}{\partial E}\right)_{E=E_F} \quad (6)$$

A sharply changing DOS implies the increased influence of carriers having relatively flat dispersion behavior, thus the origin of the increase in thermopower could alternatively be thought of as increase in the carrier effective mass (see eqn (2)). It is well known that low-dimensional, quantum-confined systems exhibit sharp, nearly dispersionless bands (Fig. 6), and appropriate size tuning to place these bands near the Fermi level could enable a marked increase in thermopower. Although this approach appears promising for enhancing ZT, quantum confinement can be difficult to achieve due to the small confinement length requirements in many materials, potentially limiting the ability of this route to enhance ZT. However, as mentioned above, similar approaches in bulk materials involving the introduction of dopants having appropriate resonant levels appear to have been more successful.

Classical size effects,[48] such as enhanced phonon scattering on surfaces and at interfaces in nanomaterials, can also be exploited through the incorporation of nanostructures to scatter heat-conducting phonons without reducing electronic conduction. For many years, the lowest thermal conductivities were measured in alloy materials, which effectively scatter high energy phonons whose wavelengths are on the same length scale as the interatomic distances in the alloy. Consequently, the concept of the 'alloy limit' was developed, which until recently was believed to represent the lowest achievable thermal conductivity in crystalline materials.[49] However, the use of nanoscale morphologies has allowed the alloy limit to be surpassed. Phonons are comprised of an approximately even distribution of wavelengths, hence, the incorporation of defects and structures covering a range of length

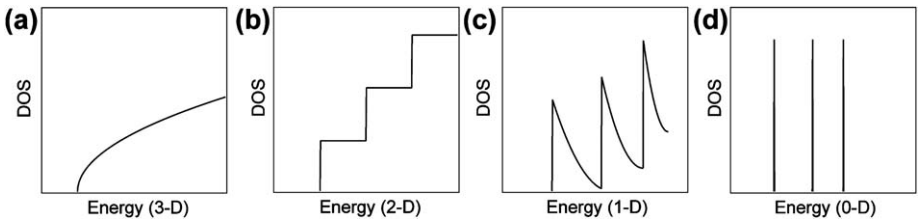

Fig. 6 Schematic illustration of the density of states (DOS) as a function of energy for: (a) a bulk material (3-D), (b) a quantum well (2-D), (c) a nanowire (1-D), and (d) a quantum dot (0-D). The DOS at the band edge increases with decreasing dimension.

scales can effectively scatter phonons of short, medium, and long wavelengths, without decreasing the electron mean free path.

Nanoscale thermoelectric enhancement due to quantum and/or classical size effects has been predicted or experimentally demonstrated for quantum dot and thin film superlattices, nanowires and nanotubes, and nanocomposites. In most cases, classical size effects derived from increased interface density appear to be responsible for the enhancements, which will be detailed in the next section. Before that, we first provide a brief overview of the various synthetic routes to nanoscale and nanostructured materials and the challenges associated with their property characterization.

3.1 Synthesis of nanostructured and nanoscale thermoelectric materials

The synthetic conditions and processing methods used to make thermoelectric materials directly affect the micro- and nanostructure, defect and impurity concentrations, and surface morphologies greatly influencing their resultant thermoelectric properties. The high surface-to-volume ratios of nanomaterials make such materials more dependent upon surface properties than bulk materials. A clear understanding of how nanostructure affects the thermoelectric properties of a material is essential for the rational design of high ZT thermoelectrics.

High quality thin films, thin film superlattices, and self-assembled quantum dot (QD) superlattices are frequently grown using molecular beam epitaxy (MBE) or electron beam evaporation of high purity source materials, giving precise control of film thickness with low levels of impurities. Nanowires can be synthesized using a variety of solution or vapor growth methods, *via* vapor–liquid–solid (VLS),[50] vapor–solid–solid (VSS),[51] or screw dislocation-driven[52] growth mechanisms or *via* template-directed[53] nanowire growth. For thermoelectric applications, epitaxially-aligned arrays of nanowires could provide direct contact with the growth substrate and facilitate nanowire tip contact during device fabrication. Non-aligned vapor grown or solution grown nanowires are less easily integrated into nanowire-based thermoelectric devices, but may be incorporated into nanocomposites using densification techniques. A variety of nanoparticle morphologies composed of many classes of semiconductor materials[54] can be chemically synthesized out of colloidal solutions and used as precursors for preparing nanocomposites.

Various methods have been employed for the synthesis of bulk nanocomposites[21] including spontaneous nanophase formation during quenching of eutectic melts and compaction of ball-milled nanopowders or melt spun materials. They have also been prepared using chemically synthesized nanoparticles, nanowires, nanotubes, or various other nanomorphologies. A densification step such as hot-pressing or spark plasma sintering (SPS) is used to achieve high density and improve electrical conductivity between particles. These common bulk metallurgical methods make nanocomposites highly scalable and inexpensive to manufacture, although precise control over structure is limited. Well-ordered nanocomposites with endotaxial quantum dots can be obtained *via* spontaneous nanophase segregation during MBE growth of thin films, but these have limited commercial potential because of the high costs and small scale of MBE synthesized thermoelectrics. While high ZT has been demonstrated with multiple nanoscale morphologies, the cost and scale of manufacture will ultimately determine which morphologies are practically feasible for each type of thermoelectric application.

3.2 Property characterization of nanostructured and nanoscale thermoelectric materials

Great care must be taken during the design and implementation of thermoelectric measurements to ensure the accuracy of the property characterization results. Furthermore, the interdependence of the thermoelectric properties means that it is important to measure the transport properties used to calculate ZT on a single sample. Calculation of ZT from the 'best' measurements taken from different samples can lead to overestimation of ZT. Further, good measurement practices include verification of results on multiple samples and different regions of a sample when possible. Electrical and thermal transport measurement of nanomaterials is quite challenging due mainly to unusual sample morphologies and small size scales. Ideally, electrical conductivity measurements are carried out using standard four-probe or van der Pauw configurations, while Seebeck coefficient measurements are carried out using the standard two-probe measurement, taking into account any thermoelectric voltage developed across sample leads.[55] Electrical contact can be difficult to achieve for some nanoscale morphologies,[56] and submicron lengthscales dictate that temperature gradients must also be quite small. Despite such difficulties, these standard techniques can be readily adapted to measuring the electrical transport properties of most nanomorphologies.

Measurements of the thermal conductivity are perhaps the most difficult for nanomaterials. In bulk materials, the common method of measuring the thermal conductivity is the laser flash method,[57] wherein a disc-shaped sample is locally heated with a laser pulse on one face while the temperature is monitored as

a function of time on the opposite face. The thermal diffusivity, and thus the thermal conductivity, can be obtained from the time-dependent temperature profile. This technique is also applicable to thin films with a few modifications. The 3ω method[58] is often the measurement of choice for the thermal conductivity of thin films. In this technique, a line of metallic material is evaporated onto the surface of the specimen to serve as both a line heater and a resistance thermometer. An AC current of frequency ω is applied to the heater line, resulting in Joule heating of the material below the heater line and generating a measureable resistance change in the thermometer, both at a frequency of 2ω. The thermal conductivity of the material can then be determined from the third harmonic of the AC voltage signal, 3ω, hence the name of the technique. Between these two techniques, most forms of nanostructured and nanoscale materials can be measured, but neither is readily applicable to the measurement of thermal conductivity in one-dimensional nanowire materials.

Measurements of the properties of single nanowires,[59–62] nanoribbons,[63] nanotubes,[64,65] and other free-standing nanostructures[66] are difficult. They can suffer from low statistical precision and reproducibility if not carried out properly. However, recently a four-probe method that allows complete transport and crystallographic measurement to be obtained from a single nanostructure has been developed.[65,67] This new method improves upon the classical thermal potentiometer setup[57] to remove the thermal contact resistance from thermal conductivity measurements and enable the complete characterization of individual nanostructures. In this technique, a nanostructure is suspended across a micro electromechanical (MEMS) device (Fig. 7) prefabricated with Pt serpentine heating coils which also act as resistance thermometers.[62] The randomly dropcast nanostructures are usually "glued" in place *via* electron beam assisted decomposition of cyclopentadienyl trimethyl platinum, ensuring better electrical and thermal contact. Probes allow the transport properties and thermopower to be measured, and a small hole in the center of the device allows high resolution electron microscopy and electron diffraction to be performed on the same nanostructure. Due to the anisotropic properties of many thermoelectric materials, knowledge of the crystallographic orientation during transport measurements is essential but has been lacking in many measurements of nanostructures. A significant advantage of the measurement setup above is that it can allow the measurement of all transport properties used to calculate ZT and the simultaneous determination of the crystal structure on a single nanostructure object.

The incorporation of many independent but effectively thermally isolated nanostructures into a composite material, such as a nanowire array embedded in a SiO_2 or Al_2O_3 dielectric matrix, produces a class of materials which are particularly difficult to characterize. This morphology only allows for two contacts on the device, thus electrical and thermal contact resistances are unavoidable in such systems. With careful device fabrication, these resistances may not dominate device behavior.[68] Further, it is impossible to know how many of the nanowires in the array one has properly made contact with,[69,70] thus error in the total nanowire cross-section involved in conducting heat or electrons is inevitable. The ZT derived from such measurements are quite susceptible to error.

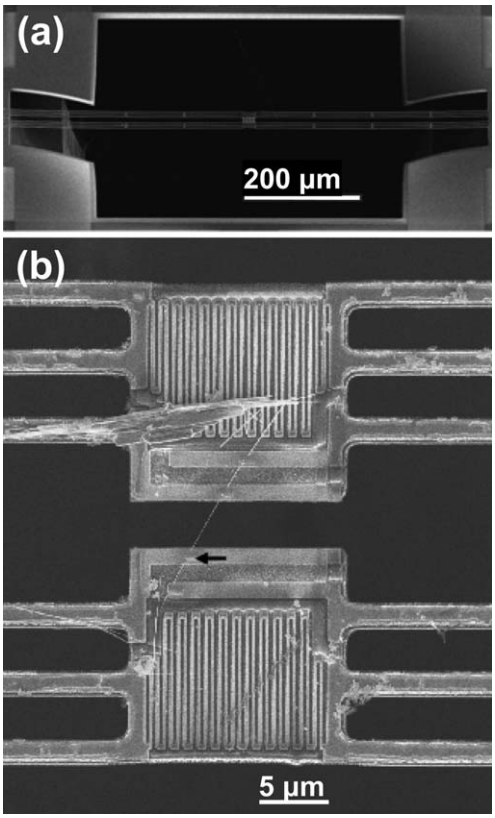

Fig. 7 (a) An electron microscope image of a MEMS device used for the measurement of nanowire thermal conductivity and other transport properties. (b) Enlarged view of (a), showing a $CrSi_2$ nanowire suspended across the device. Reproduced from ref. 62, the American Chemical Society.

4. ZT enhancement in thin films and thin film superlattices

4.1 Thin films—theory

Bismuth telluride, a well-studied material with good bulk ZT, has served as the model for many of the calculations examining how quantum confinement affects the thermoelectric figure of merit. In 1993, Dresselhaus *et al.* suggested that ZT could be increased in two-dimensional (2-D) Bi_2Te_3 quantum well structures due to confinement of electronic wavefunction in the interlayer direction, enhancing the thermopower through an increase in the DOS near the Fermi level.[17,18] Compared to the bulk three-dimensional (3-D) case, in which the chemical potential could be optimized by chemical doping only, their calculations also suggested that the chemical potential and ZT in the 2-D system could be tuned by varying the Bi_2Te_3 layer thickness (Fig. 8). They further proposed that the interfaces between layers would scatter phonons strongly, provided the Bi_2Te_3 layer thickness was less than the phonon mean free path, thus reducing the thermal conductivity as well. Work by other theorists examining phonon confinement confirmed increased interface scattering could enhance thermoelectric performance, with calculations suggesting a three- to four-fold reduction in the phonon group velocity and an increased phonon scattering rate could be achieved in Bi_2Te_3 quantum well structures.[71] Sofo and

Mahan extended this model to account for the finite probability of electron tunneling between quantum wells in Bi_2Te_3 superlattice structures.[72] They found that the critical parameter for increasing ZT was the superlattice period, rather than the thickness of the quantum well layer, predicting enhanced ZT for superlattice periodicities down to 50 Å. Below this periodicity a reduction in ZT due to energy level mixing from electron tunneling between Be_2Te_3 layers was predicted. Therefore, the thickness of the barrier layer in superlattices must be optimized to reduce parasitic heat transfer while preventing electron tunneling across the barrier. Such complications not withstanding, theoretical studies have predicted ZT improvements upwards of a factor of 6 purely by using a thin film geometry.[18]

4.2 Thin films—experiment

There have been many reports of enhanced thermoelectric properties in 2-D thin films and quantum well structures.[9,73–75] Multiple quantum well/barrier PbTe/$Pb_{1-x}Eu_xTe$ structures demonstrated experimentally that the factor S^2n could be increased by up to a factor of three relative to bulk as the PbTe layer thickness decreased, in agreement with earlier calculations.[76] The factor S^2n was introduced in this work as a more suitable measure of performance than the power factor, since both the thermopower and carrier concentration better reflect intrinsic materials parameters. The power factor is altered by both intrinsic and extrinsic parameters, as the electrical conductivity is related to the carrier mobility, and carrier mobility is determined in part by material defects. Enhanced thermopower was also seen in a *n*-PbTe/*p*-SnTe/*n*-PbTe quantum well.[77] An oscillatory dependence of the carrier concentration, electrical conductivity, and thermopower were observed in both *n*-PbTe/*p*-SnTe/*n*-PbTe quantum wells and thin PbS films.[77,78] It was proposed that the oscillations in the PbS films (which ranged from 2 to 200 nm in thickness) arose from quantum confinement, which would be expected when film thickness approaches the exciton Bohr radius (20 nm for PbS).[79] Two explanations for the oscillations of the transport properties (Fig. 9)[74] have been proposed. The phonon scattering cross-section can be defined for both the classical and quantum regimes. For sizes in between these regimes, the scattering cross-section is not well defined and an oscillation of the scattering cross-section is seen, which can manifest itself in the transport measurements.[80] Alternatively, it has been suggested that the presence of minigaps in the DOS may account for the oscillatory behavior of the thermopower and electrical conductivity.[74,81,82]

The thermal conductivity of Bi_2Te_3/Sb_2Te_3 superlattices, with sufficiently small periods ranging from 50–60 Å, achieved values below the alloy limit in superlattice thin films.[83] The reduction was independent of the individual layer thickness, provided the superlattice period was less than 60 Å. Sharp interfaces between superlattice layers are necessary to maximize ZT, since compositional grading at the alloy-like interfaces results in more modest ZT enhancement.[73]

The promising increases in ZT shown in thin films and thin film superlattices suggest that exploitation of quantum and classical size effects may allow high thermoelectric efficiency to be realized. These demonstrated improvements combined with thin film processing techniques already used in the manufacture of computer chips make it likely that thin film devices will find use in small scale applications, such as on-chip cooling.[84]

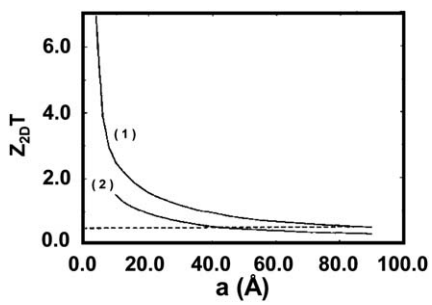

Fig. 8 Calculated ZT as a function of layer thickness (a) in a quantum well structure for layers parallel to the a-b plane (1) and layers parallel to the a-c plane (2). The dashed line corresponds to the optimized ZT for bulk Bi_2Te_3. Reproduced from ref. 17, the American Physical Society.

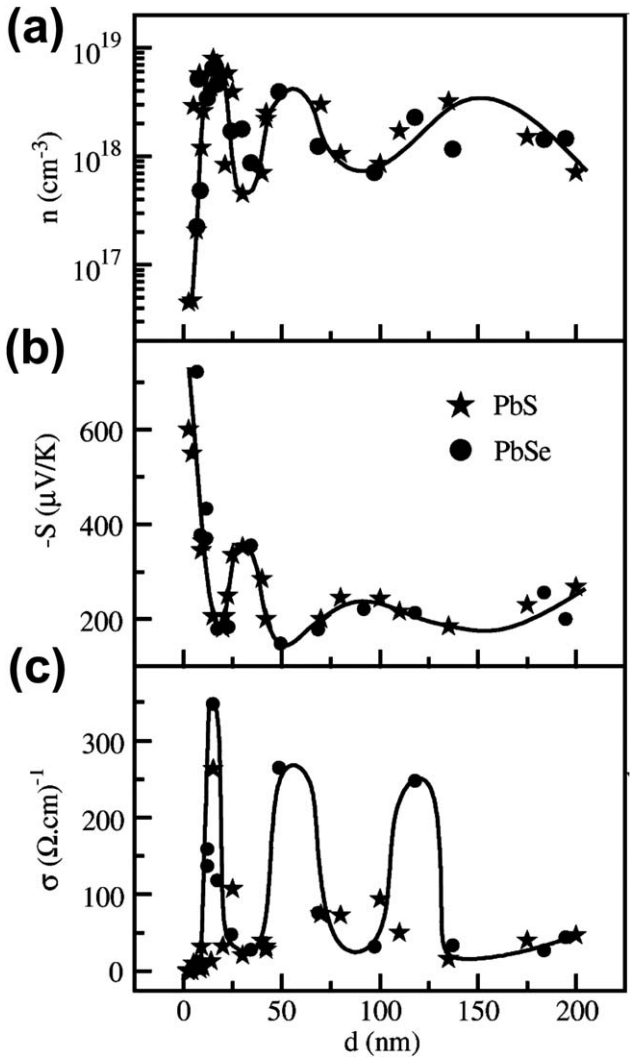

Fig. 9 Oscillation of the (a) carrier concentration (n), (b) thermopower (S), and (c) electrical conductivity (σ) as a function of quantum well layer thickness for PbS (stars) and PbSe (circles). Reproduced from ref. 74, Elsevier.

However, the high cost and low scalability of thin films limit their use in large-scale power generation and heating/cooling applications.

The efficiency of quantum well devices could suffer due to the parasitic heat loss from thermal conduction in the electrically insulating layers, which do not contribute to the power factor. Even if barrier layers with very low thermal conductivity could be found, interface modes between the layers, which run parallel to the temperature gradient, are expected to play an important role in parasitic thermal conduction.[85] The effect of material strain on the thermoelectric performance of thin film lattices presents an additional challenge. It is known that the presence of strain can reduce the degeneracy of conduction bands *via* an increase (or reduction) of the energy in different crystallographic directions, changing the mobility and conductivity of charge carriers.[86] The presence of strain can additionally change the barrier height of quantum well structures, enhancing quantum confinement and affecting the rate of electron tunneling between layers.

5. *ZT* enhancement in one-dimensional nanomaterials

5.1 One-dimensional nanomaterials—theory

Following the prediction of enhanced *ZT* in 2-D thin films, Hicks and Dresselhaus extended their model to describe one-dimensional (1-D) nanowire systems, suggesting even greater increases in the thermoelectric performance could be attained in 1-D systems due to stronger confinement and increased phonon scattering as the surface-to-volume ratio is increased.[19] For example, a four- and six-fold *ZT* enhancement in 5 nm diameter PbSe/PbS and PbTe/PbSe superlattice nanowires, respectively, was predicted.[81] An oscillatory behavior of the thermopower and electrical conductivity as a function of the Fermi levels arising from energy sub-bands in the quantum confined nanowires for very small superlattice segment length was also predicted. Both positive and negative values of the thermopower were predicted for both p-type and n-type nanowires depending on superlattice segment length. Optimal superlattice nanowire diameter and segment lengths were found, with *ZT* increasing as segment length decreased, until the *ZT* expected for the alloy limit was reached at very small segment lengths. The incorporation of unequal superlattice segment lengths for the constituent materials was predicted to enhance *ZT* further.

More recently, it has been proposed that the electric field effect[87] (EFE) could be used to enhance thermoelectric properties of nanowires by inducing carrier quantum confinement to modify the DOS at the Fermi level.[88] Calculations based on this non-chemical method to change the carrier concentration of Bi_2Te_3 nanowires predict that a room temperature *ZT* as high as 3.4 is possible when an external electric field is applied perpendicular to the nanowires. Although the calculations neglected any negative impact the nanowire surface roughness may have on carrier transport and might be an overestimation, this may present a new approach for *ZT* enhancement which deserves further investigation.

A very recent theoretical work[89] highlights potential practical limits of power factor enhancement in large scale thermoelectric devices based on nanowire composites. These calculations, based on the Landauer formalism, focus on the effect of dimensionality on the power factor and agree with previous assertions that quantum confined nanowires are more efficient thermoelectric elements than their thin film and bulk counterparts. The authors also point out the importance of the interaction between quantum wires and calculate the fill factor requirements to observe improved device behavior. Their results indicate that quantum confinement certainly produces significant (~50%) improvement in the power factor due to more efficient use of conduction channels, but the need to incorporate many such quantum wire elements into an insulating matrix will require filling factors near unity to see a gain on bulk size scales. Since filling factors between 0.25 and 0.33 are required to prevent significant coupling between individual nanowires, any power factors gains expected from quantum confinement are effectively eliminated by practical fabrication requirements.

After two recent reports (detailed later) of silicon nanowires exhibiting greatly enhanced *ZT* relative to bulk silicon,[13,14] modeling of *ZT* in silicon nanowires with a rough surface suggested $ZT > 3$ might be possible for nanowires with growth in the <111> direction.[90] Smooth nanowires were also predicted to exhibit enhanced *ZT* with decreasing diameter, due to strong surface scattering of phonons. Growth direction was seen to influence *ZT via* anisotropic phonon dispersion, with lattice heat conduction in the <110> direction projected to be twice that in either the <100> or <111> directions.[91]

5.2 One-dimensional nanomaterials—experiment

Bi nanowires have been intensely investigated due to the semimetal-to-semiconductor transition that is predicted to occur when the radial dimension is confined.[92] Long, single-crystal Bi nanowires are difficult to fabricate, hence, they are often synthesized in the pores of anodic aluminium oxide (AAO) or quartz (SiO_2) templates.[69] It has been reported that Bi nanowire arrays with diameters between 9 and 15 nm synthesized in porous SiO_2 or Al_2O_3 showed an increase in the thermopower by two to three orders of magnitude in the 100–300 K temperature range.[93] The *ZT* could not be calculated for this sample because the exact volume fraction of Bi in the templates could not be determined. It is likely that parasitic heat transfer in the electrically insulating templates could offset any enhancement of the thermopower resulting in little or no improvement in *ZT*. However, if parasitic heat transfer could be overcome, *ZT* enhancement would be expected due to the S^2 dependence of *ZT* on the thermopower. Low thermal conductivity matrixes have been investigated as a solution to parasitic thermal conductivity. The thermal conductance of an InAs nanowire array embedded in PMMA was measured using time domain thermoreflectance (TDTR).[94] Using the measured thermal conductivity of PMMA ($\approx$ 0.2 W/m·K) and the InAs/PMMA composite conductance, the thermal conductivity of the InAs nanowires was extracted from the finite-element method (FEM) model. The InAs nanowire thermal conductivity (5.3 W/m·K) was smaller than in bulk InAs by almost a factor of five, and was in agreement with the previous measurement of a single InAs nanowire.[95]

Measurement of the transport properties of nanowires with diameters larger than the Bohr exciton radius, which would not

be expected to show transport enhancement due to quantum confinement effects, have been successfully performed on $CrSi_2$ nanowires with the measurements in good agreement with the bulk values.[62] However, the thermoelectric properties of some nanowires composed of materials that have decent ZT in bulk, such as Bi_2Te_3 or InSb, are unexpectedly lower than the corresponding bulk materials.[59,61,94,96] The reason for this is not fully understood, but may be due to the limited ability to control dopant and impurity concentrations in nanowires,[59,96] and unintentional doping resulting from surface oxidation.[61] High quality nanowires of these materials are generally quite challenging to synthesize.[97] It has been suggested that nanotubes may have lower thermal conductivity than nanowires due to additional phonon scattering on the inner and outer nanotube surfaces, based on measurements of Bi_2Te_3 nanowires and nanotubes.[98,99]

Likely the most impressive demonstrations of ZT enhancement in nanostructure systems have come from studies of silicon nanowires which showed that the thermoelectric performance could be increased by up to two orders of magnitude.[13,14] These results are remarkable because bulk silicon, which has a very high thermal conductivity (142.2 W/m·K at 300 K),[100] is an rather poor thermoelectric material with the ZT of degenerately doped bulk silicon calculated to be approximately 0.01 at 300 K.[101] If similar improvement in thermoelectric performance can be demonstrated for materials that already have good bulk thermoelectric performance, ZT large enough to compete with conventional power generation and refrigeration technologies might be realized.

Hochbaum *et al.* reported $ZT = 0.60$ at room temperature for 50 nm diameter silicon nanowires with rough surfaces synthesized *via* electroless etching (EE), representing a sixty-fold increase in ZT compared to bulk Si.[14] It is believed that the high surface roughness inherent to nanowires synthesized by EE contributed to the enhanced ZT by scattering phonons on the nanowire surface, with an additional contribution to phonon scattering by point defects. To verify that the surface roughness was responsible for the thermal conductivity reduction, smoother silicon nanowires of similar diameter were grown *via* VLS growth for comparison. The thermal conductivity of the EE-grown nanowires of a given diameter was reduced by an order of magnitude compared to VLS-grown nanowires, supporting a connection between surface roughness and lower thermal conductivity.

Boukai[13] *et al.* reported values of ZT as high as 1 at 200 K for silicon nanowires fabricated *via* the superlattice nanowire pattern (SNAP)[102] transfer process. The enhancement in ZT was reported to be the result of a marked reduction in the thermal conductivity coupled with an enhanced phonon drag contribution to the thermopower. Although the surfaces of these nanowires did not exhibit a high degree of surface roughness, the high surface-to-volume ratio of these 20 nm diameter nanowires appeared to scatter phonons efficiently, as evidenced by lower thermal conductivity with decreasing wire diameter.

Recent advances in the synthesis of nanowires of metal silicides,[103] have opened up the possibility of combining nanowire morphology with a complex crystal structure. Single-crystal nanowires of $Mn_{19}Si_{33}$, a commensurate Nowotny chimney ladder structure (see section 2.3), have been successfully synthesized.[39] Phonon confinement could occur more readily in these silicide nanowires with a level of structure complexity rarely observed in common semiconductors (unit cells parameters above 10 nm and higher), which together with surface roughness could result in pronounced reduction of the lattice thermal conductivity. Preliminary electrical transport characterization reveals bulk-like resistivity but more thorough transport studies are underway. In some sense, these unique silicide nanostructures combine the complex structure approach in bulk materials and the nanomaterials approach and could open up new opportunities to enhancing thermoelectric properties.

At this time, large-scale synthesis of bulk quantities of nanowires at low cost and the techniques to easily integrate nanowire arrays into thermoelectric devices still need to be developed. Advancements in these areas will be required if large-scale high efficiency nanowire thermoelectric devices are to be realized.

6. ZT enhancements in nanostructured composite materials

6.1 Nanostructured composites—theory

Both heterogeneous and homogeneous nanostructured composites have been proposed to increase ZT by scattering phonons more than electrons. Preferential scattering is possible because the mfps of phonons typically range from the single nanometers up to a few hundred nanometers, whereas the carrier mfp is typically only a few nanometers.[104] Incorporation of nanostructures covering a variety of length scales is, therefore, expected to reduce the lifetime of a broad distribution of phonons while leaving charge transport largely unchanged. While nanostructures are efficient scattering centers for low to moderate energy phonons with wavelengths on the length scale of typical nanostructures, they are less effective at scattering high energy phonons (< 1 nm wavelength). Since phonon scattering is proportional to υ^4,[105] nanocomposites based on an alloy matrix may be most effective at reducing phonon lifetimes.[15,105] Impressive reductions of the phonon mfp have been demonstrated in nanostructured silicon, a material with high bulk thermal conductivity.[15,46] Values as low as 6.2 W/m·K at 300 K (compared to 142.2 W/m·K at room temperature) have been observed in homogeneous nanocomposites doped with phosphorus and gallium phosphide, to enable a maximum ZT of 0.7 to be achieved at 1275 K.[46] In addition to classical scattering effects, quantum size effects may play a role in the high ZT demonstrated by enhancing the thermopower due to carrier energy filtering.[106] Heterogeneous nanocomposites may have an advantage over homogeneous nanocomposites. High surface area nanoscale morphologies are not thermodynamically stable, due to their high surface energies, and may be prone to grain sintering and chemical diffusion during operation at elevated temperatures, although the thermal conductivity of nanostructured $Si_{1-x}Ge_x$ has been shown to be stable when samples are aged at 1275 K for longer than one year.[21] Heterogeneous nanocomposites with isolated precipitates may prove more resistant to structural changes, and hence able to maintain enhanced thermoelectric performance over time.

Modeling has proven useful for predicting the effects of reduced dimensionality in 1-D and 2-D systems. However,

nanocomposites can be quite complex making accurate modeling difficult. Even though some models have been developed, it is not always easy to fabricate nanocomposites with the predicted optimum structures using current synthesis techniques. Theoretical investigations of phonon heat transport have been carried out for nanostructured PbTe,[107] $Si_{1-x}Ge_x$,[108] metal silicide/$Si_{1-x}Ge_x$,[109] $Mg_2Si_xGe_ySn_{1-x-y}$,[110] and 2-D periodic silicon nanowires or nanotubes in a germanium matrix.[111] High interface densities appear to be the key factor for enhancing ZT, with lower thermal conductivity predicted for periodically-aligned or randomly-ordered nanocomposites (Fig. 10a) compared to 1-D superlattice systems or bulk alloys of the same nominal composition.[108,109] $Si_{1-x}Ge_x$ nanocomposites have lower thermal conductivity than the $Si_{1-x}Ge_x$ alloy of the same composition (Fig. 10b), with the staggered fcc distribution most effective at reducing phonon transport. Smaller nanoparticle size (increased interface density) similarly enhances phonon scattering (Fig. 10c). The reduction of thermal transport is predicted to be independent of precipitate morphology, with thermal conductivity decreasing as particle diameter decreases.[108–111] Indeed, thermal conductivities lower than the alloy of the same chemical composition are predicted for interface densities greater than approximately 0.10 nm^{-1}.[108]

The possibility of enhanced ZT in aligned homogeneous porous structures (Fig. 11a) has also been predicted.[111,112] For a composite with a given porosity, the thermal conductivity is expected to decrease as the pore radius decreases and interface density increases (Fig. 11b).[111] Confinement of charge carriers in two directions imposed by porous structures flattens the dispersion bands, increasing the carrier effective mass and enhancing the power factor.[112] For optimum pore wall thickness and pore periodicity, a seven-fold enhancement of the power factor is predicted, with more modest enhancements expected as the pore radius and periodicity deviate from their optimum values.

Although it is hoped that carrier transport will not be reduced in nanocomposites, in many cases the reported electrical conductivity has been lower in nanocomposites than in bulk crystals of the same nominal composition. It is well known that carrier transport is lower in polycrystalline materials than in single crystals. Therefore, a reduction of carrier transport in nanocomposites should not be surprising, and ought to be expected to be similar in magnitude to those seen in polycrystalline materials. The porosity of nanocomposites has also been shown to affect the transport properties of these materials.[113]

The thermal conductivity of a variety of metal silicides embedded in a $Si_{1-x}Ge_x$ matrix was calculated to determine which metal silicides could reduce the thermal conductivity without impacting the electron mfp.[109] Nanoparticle inclusions accounting for as little as 3.4% of the total composite are predicted to decrease the thermal conductivity by as much as 4–8 times below the value of the $Si_{1-x}Ge_x$ alloy, with the thermal conductivity decreasing as nanoparticle percentage increased (Fig. 12). A silicide-dependent optimum nanoparticle radius of less than 10 nm was found, and almost all silicide/$Si_{1-x}Ge_x$ composites with nanoparticles ranging in radius from 5 to 20 nm, including those containing $MnSi_x$, Mg_2Si, β-$FeSi_2$, and $CrSi_2$, have calculated thermal conductivities below 2 W/m·K (Fig. 12).

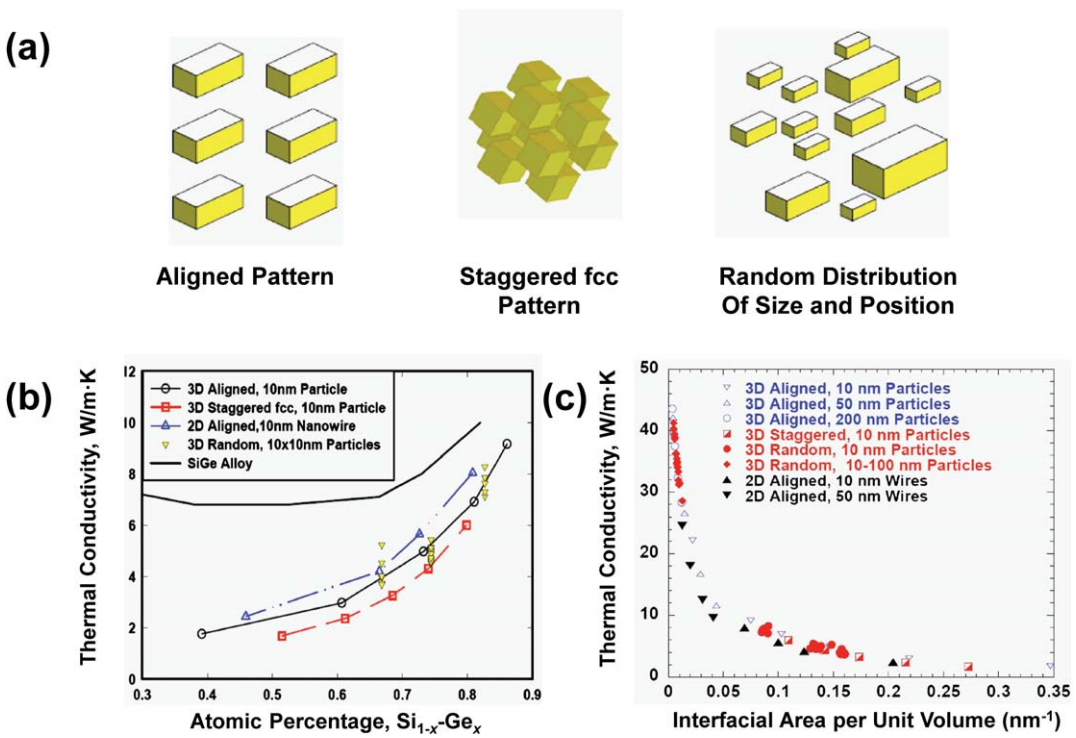

Fig. 10 (a) Schematic drawing of nanoparticle distributions in a nanocomposite, including aligned pattern, staggered fcc pattern, and random distribution of size and position, (b) calculated thermal conductivity as a function of atomic percentage x for various alignment patterns and for the bulk $Si_{1-x}Ge_x$ alloy, and (c) calculated thermal conductivity as a function of interfacial area for different size nanoparticles and alignment patterns. Reproduced from ref. 108, ASME Publications.

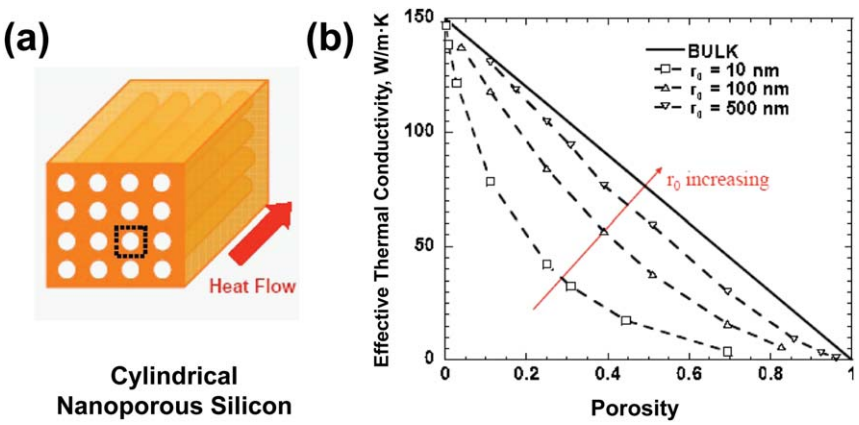

Fig. 11 (a) Nanoporous silicon with aligned cylindrical pores, with heat transport in the direction of the pore axis. (b) Effective thermal conductivity as a function of porosity for pores with different radii. From ref. 111, the American Physical Society.

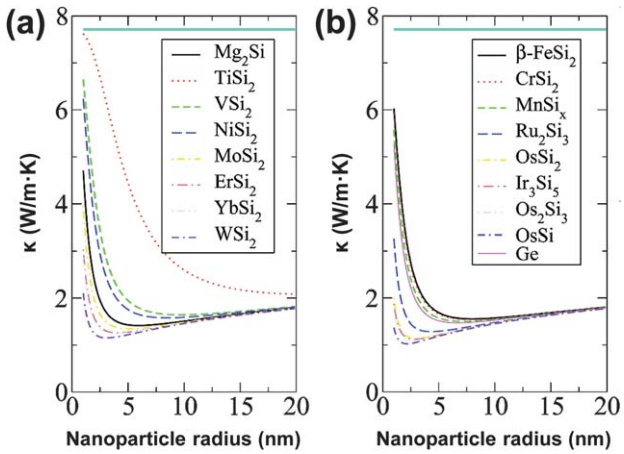

Fig. 12 Calculated room temperature thermal conductivity as a function of nanoparticle radius for nanocomposites with a fixed 3.8% silicide nanoparticle concentration in a $Si_{0.5}Ge_{0.5}$ matrix. (a) Metallic silicides, and (b) semiconducting silicides. The calculated thermal conductivity of the $Si_{0.5}Ge_{0.5}$ alloy without nanoparticles is shown as the horizontal line at the top of each graph. Reproduced from ref. 109, the American Chemical Society.

The greatly lowered thermal conductivity results in calculated *ZT*s greater than 0.5 at room temperature, with *ZT*s as high as 1.7 when extrapolated to 900 K. Similar calculations examining $Mg_2Si_xGe_ySn_{1-x-y}$ nanoparticle-in-alloy materials have predicted *ZT* of approximately 1.9 at 800 K for Mg_2Si or Mg_2Ge nanoparticles embedded in a $Mg_2Si_{0.4}Sn_{0.6}$ matrix.[110]

6.2 Nanostructured composites—experiment

There has been an explosion of recent reports on the use of nanostructured composite materials to enhance *ZT* relative to the related bulk materials. Many reports concerning the thermoelectric performance of nanocomposites focus on materials that have a high bulk *ZT*, such as the $(Bi,Sb)_2(Te,Se)_3$ and $Si_{1-x}Ge_x$ alloys, with the hope that the anticipated enhancement due to the nanostructures might yield *ZT*s sufficiently high to compete with traditional power generation and cooling technologies. Bi_2Te_3 and its alloys, which are considered the best room temperature thermoelectric materials, have a *ZT* of approximately unity.[8] The key idea is that by properly designing the nanostructures, phonons are effectively scattered but electrons are not; therefore, thermal conductivity is suppressed with the hope of preserving the electrical properties.

The nanoscale morphology of nanostructured composites appears to be dictated primarily by interface energy minimization and material stress relief.[114] To date, no clear consensus has arisen regarding which types of precipitates may be most beneficial or detrimental to thermoelectric performance. Quantitative analysis is difficult to perform due to the wide variety of precipitate and inclusion types present in nanocomposites, thus only qualitative analysis with respect to how nanostructure may alter thermoelectric performance has been reported. As nanostructure greatly influences the transport properties, understanding how grain size, morphology, and composition influence transport is a prerequisite for the rational design of high *ZT* nanocomposites. For example, nanocomposites comprised of randomly oriented grains should demonstrate isotropic properties even when the bulk material properties are anisotropic, whereas layered or laminated structures would likely possess anisotropic thermal and electrical conductivity, with scattering enhanced or minimized based upon whether transport is orthogonal or parallel to the layers. Layered composites could perhaps behave as PGECs for transport in the direction parallel to the layers, while increased carrier scattering would be expected for transport in the cross-layer direction.

Of the variety of nanostructures seen, nanoprecipitates can be categorized based on two aspects: (1) the type of interface (sharp or diffuse) between the nanoprecipitates and the surrounding material, and (2) whether the composition of the grain and surrounding matrix are identical or differ in chemical composition. The interface type will influence the transport properties and thermoelectric performance of nanocomposites. Coherent lattices, such as that seen in Fig. 13a, are desirable to minimize electron scattering. Coherent interfaces are typically seen in MBE grown nanocomposites (due to the slow layer-by-layer crystal growth inherent to this technique) and occasionally in nanocomposites obtained *via* metallurgical methods. Phonons are strongly scattered at the interface, particularly when their wavelengths are matched to the size of the precipitates, reducing

thermal transport. The thermal conductivity of a MBE grown ErAs/$In_{0.53}Ga_{0.47}As$ nanocomposite was reduced by almost a factor of two, while the power factor improved modestly, demonstrating the ability of coherent nanoparticle interfaces to shorten phonon lifetimes without affecting the electron mfp.[115] Low angle (Fig. 13b and 13c) and high angle grain boundaries (Fig. 13d) should enhance phonon scattering further, due to more pronounced breaking of the lattice symmetry at the interface. When the matrix and nanoprecipitate compositions are similar, carrier scattering rates should resemble those in a polycrystalline material. Nanograins with diffuse interfaces, which have short range disorder, would be expected to destroy phonon coherence and reduce both the phonon and carrier mfps. Compositional inhomogeneities also affect carrier transport at the interfaces.[116] The mass fluctuations and different electronic environments make these interfaces efficient scattering centers for both phonons and charge carriers, which is undesirable.

Although researchers typically seek to minimize charge carrier scattering in the interest of maintaining high electrical conductivity and large power factor, preferential scattering of carriers at element rich/deficient regions could be beneficial for thermoelectric performance in materials displaying bipolar conductivity. For example, the enhanced ZT seen in a $Bi_xSb_{2-x}Te_3$ nanocomposite containing Bi-poor nanograins surrounded by a Bi-rich interface region a few nanometers in thickness may have been achieved in part by a reduction of the electron conductivity.[10] The presence of Bi-rich and Bi-poor regions may have created potential inhomogeneities in the interface region to scatter electrons preferentially, thus reducing bipolar conduction.[117] Bipolar conduction decreases the magnitude of the thermopower, thus preferential interfacial carrier scattering could enhance the power factor of this and similar nanocomposites.

Nanocomposites containing nanodots of pure elements have been reported in alloys of Bi_2Te_3 and in PbTe/Si eutectic composites, in which pure Te and pure Pb nanodots were present, respectively.[10,117–119] The mass difference and independent lattice of elemental precipitates may scatter phonons strongly, while electrons can also be scattered at the interface due to the extremely different matrix and precipitate electronic band structures. Incorporation of an alloy into eutectic composites has been reported to enhance ZT even further; for example, an n-type PbTe-Si(8%) eutectic demonstrated $ZT = 0.9$ at 675 K, and the eutectic PbTe-$Ge_{0.8}Si_{0.2}$(5%) showed ZT as high as 1.3 at 778 K.[118,119]

Nanocomposites comprised of an amorphous matrix containing nanocrystalline precipitates have also been infrequently reported.[120,121] The electrical conductivity of amorphous/crystalline composites was found to be two orders of magnitude lower than polycrystalline materials of the same chemical composition; however, the power factors are only modestly lower, suggesting an enhancement of the thermopower must occur. If the thermal conductivity can be sufficiently reduced, enhanced ZT may be possible for amorphous/nanocrystalline composites.

The most likely new thermoelectric nanomaterials to be commercially viable in the near future are nanocomposites. These materials have already shown significant improvements in thermoelectric performance over their bulk counterparts, and many can be produced *via* relatively inexpensive processing techniques. In the following section, we will survey the reported thermoelectric properties of nanostructured composites, focusing on material families.

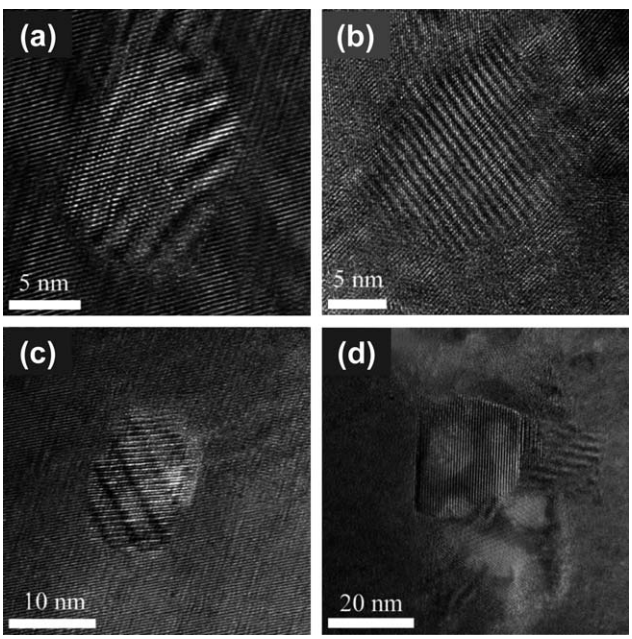

Fig. 13 High resolution TEM images of precipitates in a $Bi_xSb_{2-x}Te_3$ nanocomposite. (a) Coherent Sb-rich precipitate, (b) precipitate with a low-angle grain boundary and same composition as the matrix, (c) Sb-rich precipitate with a low-angle grain boundary, and (d) pure Te precipitate with a high-angle grain boundary. Reproduced from ref. 117 the American Chemical Society.

6.3 Nanocomposite material families

It is worth noting that many nanocomposites share similar nanomorphology and reduced thermal conductivity, even when synthesized using different methods (for example, ball milling *versus* eutectic quenching, or MBE quantum dot superlattice *versus* chemically synthesized nanocomposites). If we assume that the carrier concentrations of these nanocomposites have been optimized, then notable variations in ZT within a material family should be due to differences in the nanostructures.

6.3.1 Bismuth chalcogenide based nanocomposites. The most notable study of nanostructure morphology examined a polycrystalline p-type $Bi_{0.5}Sb_{1.5}Te_3$ bulk alloy synthesized by hot pressing of ball-milled nanopowders. This material exhibited an $ZT = 1.2$ at room temperature and impressive ZT_{max} of 1.4 at 373 K.[10] The isotropic ZT resulted from the random grain orientation of the sample. Although the electrical conductivity was reduced somewhat, the thermal conductivity was reduced more significantly from the bulk ingot of the same material, with $\kappa_{min} \approx 1.0$ W/m·K and ≈ 1.3 W/m·K in the nanocrystalline and ingot samples, respectively. Hence the maximum ZT demonstrated in the nanocomposite was almost 30% higher than the bulk ingot. A thorough investigation of the nanostructure of this material revealed a complex polygonal grain structure (Fig. 13),

with diameters ranging from a few microns down to a few nanometers, which likely resulted in efficient scattering of a broad distribution of phonon wavelengths. In addition to the primary nanocrystalline grains often having well defined grain boundaries, Sb-rich nanodots ranging from 2 to 10 nm in diameter with diffuse boundaries and pure Te precipitates with diameters between 5 to 30 nm were also observed.[10,117] Significantly, the authors compared the thermoelectric performance of this nanocomposite against a bulk Bi_2Te_3-based commercial thermoelectric element by fabricating two thermoelectric cooling devices, each with a commercial n-type Bi_2Te_3 leg and with the p-type leg made of either the nanocomposite or a commercial p-type Bi_2Te_3 leg (Fig. 14a). The nanocomposite device produced temperature differences up to 20 degrees greater than the device with a commercial p-type leg (Fig. 14b), definitively demonstrating the improved efficiency of this nanocomposite material.

Other Bi_2Te_3 based nanocomposites have shown performance similar to bulk Bi_2Te_3,[98,119] while still others have performed poorly in comparison.[122] Reduction of grain size and incorporation of nanostructures have increased the thermoelectric performance for some Bi_2Te_3 based nanocomposites,[10,117] but there exists a wide variation in the magnitude of ZT (ranging from approximately 0.4 to 1.7) reported for composites having similar nominal compositions. It is clear that the details of the nanostructures and the preparation must have a large impact on nanocomposite thermoelectric performance.

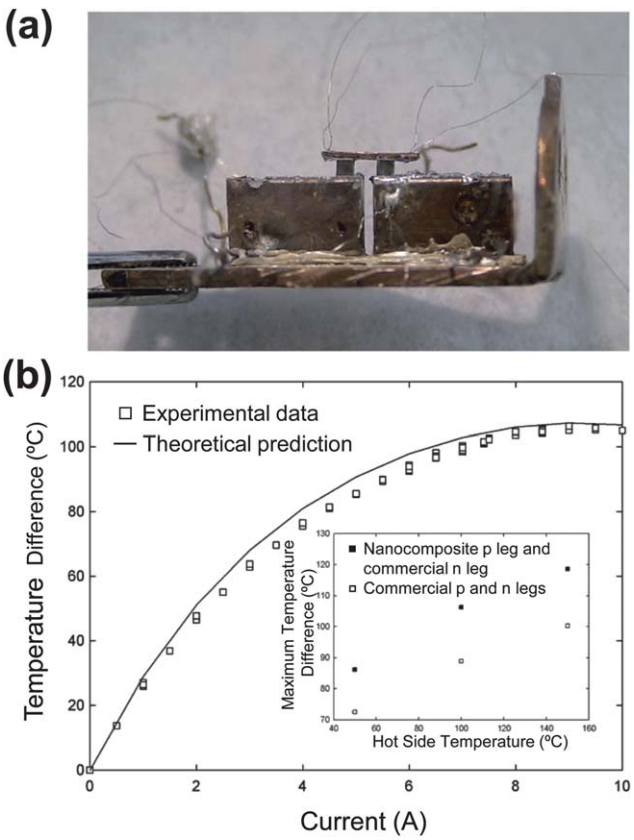

Fig. 14 (a) Photograph of a thermoelectric device using a bismuth antimony telluride nanocomposite p-type leg and a commercial n-type leg. (b) Measured temperature difference as a function of current for the device pictured in (a), and comparison of the measured maximum temperature difference of two separate devices (inset), having commercial n-type legs and either the nanocomposite p-type leg (closed squares) or a commercial p-type leg (open squares). Reproduced from ref. 10, Science/AAAS.

$ZT = 1.47$ was reported for nanocomposite synthesized by hot pressing of a 1 : 1 mixture of Bi_2Te_3 and Sb_2Te_3 nanopowders with diameters below 20 nm.[123,124] The laminated structure of this nanocomposite after hot pressing was composed of nanolayers with thicknesses ranging from 5 to 50 nm, with both Bi_2Te_3 and Sb_2Te_3 layers identified using X-ray diffraction. Because the nanocomposite was not intentionally doped, it may be assumed that optimization of carrier concentration could allow even higher ZT to be achieved. Bulk amorphous p-type $Bi_{0.52}Sb_{1.48}Te_3$ with 5 to 15 nm diameter nanocrystalline precipitates produced *via* melt spinning (MS) and spark plasma sintering (SPS) exhibited $ZT = 1.56$ at 300 K, with the enhancement primarily resulting from increased phonon scattering, which reduced the thermal conductivity to approximately 0.7 W/m·K.[121] The unusual coexistence of both amorphous and nanocrystalline phases is believed to result from the large temperature gradient between the contact and free surfaces. A similarly synthesized Pb-doped $(Bi,Sb)_2Te_3$ nanocrystalline composite with grains typically less than 10 nm in diameter demonstrated a thermal conductivity of approximately 1.2 W/m·K and $ZT > 1$ at about 435 K, similar to bulk Bi_2Te_3 alloys.[125] The lack of thermoelectric enhancement suggests that this nanocomposite, which did not contain an amorphous matrix, was less effective at reducing phonon lifetimes.

6.3.2 Lead chalcogenide based nanocomposites. The highest reported ZT for a lead chalcogenide based nanocomposite was observed in a Bi-doped n-type PbSeTe/PbTe quantum dot superlattices (QDSL) comprised of PbSe nanodots in a PbTe matrix fabricated by MBE, with claimed $ZT = 3$ at 550 K and $ZT = 1.6$ at 300 K, yielding a cooling power 40% higher than bulk $(Bi,Sb)_2(Se,Te)_3$.[126,127] Another series of QDSLs based on the PbSeTe/PbTe system with reported ZTs ranging from approximately 1.15 to 1.7 for various dopant levels and growth conditions.[127] Although these reported ZTs are quite impressive, the MBE fabrication process is not easily scaled up. The growth time required to fabricate each approximately 100 μm thick QDSL at the reported rate of 1.0 to 2.0 μm/h is two days *per device*,[126] much too slow and expensive for large-scale thermoelectric devices. The relatively large increases in ZT reported for QDSL compared to metallurgical methods likely results from low defect densities, as the slow growth of MBE allows surface diffusion of atoms and typically yields high quality films with coherent inclusions, but at a cost of reduced throughput and higher production costs.

An attempt to use Cd-substitution to introduce resonant levels into PbTe to enhance the DOS near the Fermi level was unsuccessful, however, nanostructuring resulting from the low solubility of Cd in PbTe decreased the thermal conductivity markedly to approximately 0.5 W/m·K to give $ZT \approx 1.2$ near 720 K.[128] Enhanced thermopower was also reported when both Pb and Sb nanoprecipitates were present in a PbTe matrix (but not when only Pb or Sb nanoprecipitates were present), resulting in an apparent increase in the carrier mobility to give $ZT = 1.4$ between 650–700 K.[129]

Recently, a series of complex nanostructured materials that undergo nanophase segregation to form nanoparticle-in-an-alloy materials based on PbTe, Bi_2Te_3, and PbSb alloys have been extensively investigated as enhanced ZT materials.[24] A high ZT of about 2.2 was reported for a complex PbTe-based alloy $Ag_{1-x}Pb_{18}SbTe_{20}$ (lead antimony silver telluride, LAST) melt-grown sample.[12] Although precipitates had been seen in the LAST compounds even 40 years ago and deviations between the measured thermal conductivity and theoretical calculations were observed, these precipitates had been seen as defects in the crystal and the low thermal conductivity had been explained in terms of alloy point defect scattering.[130] Evidence suggests that the LAST alloys are not true solid solutions, but in fact are complex nanostructured composites containing Ag-Sb-rich inclusions, particularly when deviations from the ideal stoichiometry are seen.[12,131] The compounds spontaneously phase segregate to form nanoscale domains within the solid matrix. Nanodots embedded within the bulk alloy were found with TEM analysis, suggesting that nanostructuring as well as simple alloy behavior played a role in reducing the thermal conductivity to about 2.3 W/m·K at room temperature to enhance ZT. Lower ZT (approximately 1) was reported for a hot pressed ball milled LAST nanocomposite ($Ag_{1-x}Pb_{18}SbTe_{20}$), suggesting that stoichiometry, processing conditions, relative density, and lattice strain may play important roles in the thermoelectric performance.[113,132] A number of other complex nanostructured alloys, including the tellurium-antimony-germanium-silver (TAGS) and potassium-lead-antimony-tellurium (PLAT) alloys have also exhibit reduced thermal conductivity and high ZT with reported maximum ZT of approximately 2.2 and 1.6, respectively.[133]

6.3.3 Silicon-germanium alloy based nanocomposites. Bulk $Si_{1-x}Ge_x$ alloys already have fairly high ZT, having a maximum reported for p- and n-type ZT of approximately 0.7 and 1, respectively, for germanium contents between 20–30%.[32,134] The use of nanostructuring to enhance phonon scattering has allowed ZT as high as 0.95 to be obtained near 1100 K in p-type alloys.[11] It was reported that prolonged annealing of the $Si_{1-x}Ge_x$ nanocomposite at 1373 K for 7 days did not lead to noticeable grain sintering, suggesting that the nanocomposite may be stable in the operating temperature region. Further, the thermal conductivity of $Si_{1-x}Ge_x$ nanocomposite was stable when annealed at 1275 K for over a year.[21] An alloy containing only 5% germanium ($Si_{95}Ge_5$) demonstrated thermal conductivity as low as 6 W/m·K, achieving a maximum $ZT > 0.9$ at 900 K.[15] Despite the higher Si concentration in this nanostructured alloy, the thermal conductivity is on the same order as bulk $Si_{80}Ge_{20}$.[32]

6.3.4 Metal silicide based nanocomposites. Metal silicides,[135] a class of refractory intermetallic compounds formed between the metals and silicon, are particularly attractive as thermoelectric materials due to their relative low cost and the high abundance of their constituent elements in the Earth's crust compared to other commonly-used thermoelectric materials. They are not as well studied for thermoelectric applications as the more popular chalcogenide materials, but studies on bulk Mg_2Si,[136] $MnSi_{1.7}$,[38,40,137] $CrSi_2$,[138] and β-$FeSi_2$[139,140] have shown admirable ZTs of 1.1, 0.7, (Fig. 3) 0.25, and 0.6, respectively. Their lower toxicity, robustness, low cost, and elemental abundance, compared to Bi_2Te_3 and PbTe based materials, make the use of semiconducting silicides very attractive for large scale thermoelectric applications.[141]

Mg_2Si and its nanocomposites with other group IV elements have shown ZT as high as 1.1 for the $Mg_2Si_{0.4}Sn_{0.6}$ solid solution.[136] Although an investigation of possible nanostructures was not reported, a recent report suggests that the addition of a small amount of impurities (as little as $x = 0.0075$ in $Mg_2Si_{0.4-x}Sn_{0.6}Sb_x$) results in the formation of a nanocomposite.[142] The embedded nanodots reportedly reduced the lattice thermal conductivity by almost half compared to the Sb-free sample, giving $ZT \approx 1.1$ at 773 K. Nanostructured Bi-doped Mg_2Si has shown enhanced thermopower and reduction of the thermal conductivity to as low as 2.5 W/m·K with increasing grain density.[143] Consistent with increased grain boundary scattering, the electrical conductivity was seen to decrease as the average crystalline grain size decreased. The changes in transport properties overall served to enhance ZT, achieving a maximum $ZT = 0.8$ at 800 K. Nanocomposites with approximately 30 nm diameter Mg_2Si grains interdispersed with MgO was also prepared as a possible thermoelectric material.[144] This composite was synthesized in a solid state gas displacement reaction using magnesium vapor to convert nanostructured SiO_2 in the form of diatomaceous earth. This method could potentially be expanded to synthesize other thermoelectric silicide nanocomposites with small grain sizes and high interface density.

The higher manganese silicides (HMS), which naturally form bulk composites with MnSi when synthesized *via* bulk crystallization due to the peritectic nature of the HMS phase,[38] have also been investigated in nanocomposites with Ag_2Te or PbTe.[145] Although the thermal conductivity was decreased and thermopower increased in these nanocomposites, observed ZT was lower due to severely decreased electrical conductivity. It is likely that the simple method used in the preparation of this composite (hand-milling the bulk powders followed by hot-pressing) and high porosity of the pressed samples contributed to the poor performance. HMS nanowires were recently synthesized for the first time[39] and may be a model system to study the how convergence of complex crystal structure and nanomorphology impact thermoelectric properties. The chemistry already developed for nanowire synthesis[103] could also be useful for preparing nanoparticles of silicides, both of which are useful materials for preparing nanocomposites.

Sputtered films of silicon-rich Cr_xSi_{1-x} showed increasing thermopower as the chromium content decreased.[146] The films, which were amorphous during sputtering, crystallized into a nanocomposite containing $CrSi_2$ and Si crystallites. Full thermoelectric characterization was not reported, so it is unknown if the presence of Si crystallites will ultimately enhance ZT in this case.

It has been suggested that incorporation of insulating inclusions within nanocomposites could also lead to an increase in ZT, provided that the inclusions are contained within the grains, as opposed to along the grain boundaries, to maintain efficient electrical conduction.[147] The results of integrating inert oxides into thermoelectric nanocomposites have been mixed. The thermal conductivity has been reduced in nanocomposites containing inert oxide phases;[147,148] however, negative impacts on carrier transport have also been reported.[147] A β-$FeSi_2$/SiO_2

nanocomposite with 4 wt% SiO_2 showed enhanced thermopower in the 400–800 K range, as well as a depressed thermal conductivity, with $\kappa_{min} \approx 3.5$ W/m·K.[140] Although the electrical conductivity was modestly decreased, the ZT reached a maximum $ZT \approx 1.2$ near 625 K. A similar nanocomposite containing 2 wt% of the conducting oxide TiO showed a ZT_{max} slightly above 1, higher than the $ZT_{max} \approx 0.6$ found for β-$FeSi_2$ alone.

6.3.5 Summary of trends in nanostructure composite materials. As can be seen in the above examples, the enhancement of thermoelectric properties in nanocomposites varies greatly between samples, *i.e.* sample preparation appears to strongly affect thermoelectric performance. While QDSL nanocomposites consistently show significantly enhanced ZT, no one bulk processing method shows a clear and consistent advantage over another in terms of achieving enhanced thermoelectric performance. The resistivity of nanocomposite samples usually increases as nanoparticle content increases, indicating that increased interface density in nanocomposites leads to additional electron scattering.[122,149] However, the marked decrease in the thermal conductivity and increased thermopower often result in a net enhancement of ZT. It has been suggested that low relative density nanocomposites should have poor electrical conductivity and power factors due to strong carrier scattering,[113] but a consistent trend correlating the relative density with the magnitude of ZT has not emerged due in part to the fact that few researchers report the relative density of their sample. In some cases, nanocomposites with low relative density have shown enhanced ZT; for example, a layered Bi_2Te_3/Sb_2Te_3 nanocomposite with a relative density ranging between 92.8 and 94.7% was reported to have a $ZT_{max} = 1.47$ at 440 K.[124] Clearly, a greater understanding of the effects of synthesis conditions and nanomorphology on material properties is still required to allow more rational design of thermoelectric nanocomposites.

7. Summary and perspectives

Reducing the size and dimensionality of thermoelectric materials has been demonstrated to increase the thermoelectric figure of merit, ZT, in nanoscale and nanostructured materials relative to their corresponding bulk materials, confirming the predicted ZT enhancement due to classical and quantum size effects. These increases result primarily from lowered thermal conductivity as interface density increases, as well as from possible quantum size effects including improved thermopower resulting from the increased electronic DOS at the Fermi level in low-dimensional systems. Although many of the highest reported ZT are for thin film and nanowire materials, the high costs and limited scalability of these methods will likely limit their practical large-scale applications. However, careful investigation of well-controlled nanowire and thin film nanomaterials will continue to provide the fundamental insights necessary to understand the effect of nanostructures on ZT enhancement. Inexpensive bulk nanocomposites have also demonstrated impressive ZT relative to bulk crystals and are expected to find use in many applications currently filled by conventional power generation and cooling technologies.

Thermoelectric performance appears to depend sensitively on both the nanostructure and synthesis conditions. At this time, there exists only a qualitative understanding of how nanostructure affects the transport properties and thermoelectric performance of these complex materials. The quality and composition of surfaces and interfaces, which can greatly influence transport properties in high surface area nanoscale materials, can be difficult to control, and may account for some of the variation between reports for a given material family and nanoscale morphology. Continued research to gain a more quantitative understanding is required to allow the rational design and preparation of nanocomposites and accelerate the wide adoption of thermoelectric technologies in power generation and cooling applications.

Acknowledgements

We thank the NSF/DOE Partnership on Thermoelectric Devices for Vehicle Applications (CBET-1048625), University of Wisconsin-Madison graduate school, the Sloan Research Fellowship, the Research Corporation through a Cottrell Scholar Award, the ACS ExxonMobil Solid State Chemistry Fellowship, and the DuPont Young Professor Grant for support. The authors would also like to thank Prof. Li Shi and Dr Arden Moore of University of Texas–Austin for fruitful discussions and collaborations on this research topic.

References

1 International Energy Outlook 2009, http://www.eia.doe.gov/oiaf/ieo/pdf/world.pdf, Accessed March 11, 2010, 2010.
2 H. J. Goldsmid, *Applications of Thermoelectricity*, Wiley, New York, 1960.
3 D. K. C. MacDonald, *Thermoelectricity: An Introduction to the Principles*, Wiley, New York, 1962.
4 L. E. Bell, *Science*, 2008, **321**, 1457–1461.
5 J. Yang and F. R. Stabler, *J. Electron. Mater.*, 2009, **38**, 1245–1251.
6 G. J. Snyder and E. S. Toberer, *Nat. Mater.*, 2008, **7**, 105–114.
7 N. W. Ashcroft and N. D. Mermin, *Solid State Physics*, Holt, Rinehart and Winston, New York, 1976.
8 F. J. DiSalvo, *Science*, 1999, **285**, 703–706.
9 G. Chen, *Adv. Sci. Technol.*, 2006, **46**, 104–110.
10 B. Poudel, Q. Hao, Y. Ma, Y. Lan, A. Minnich, B. Yu, X. Yan, D. Wang, A. Muto, D. Vashaee, X. Chen, J. Liu, M. S. Dresselhaus, G. Chen and Z. Ren, *Science*, 2008, **320**, 634–638.
11 G. Joshi, H. Lee, Y. Lan, X. Wang, G. Zhu, D. Wang, R. W. Gould, D. C. Cuff, M. Y. Tang, M. S. Dresselhaus, G. Chen and Z. Ren, *Nano Lett.*, 2008, **8**, 4670–4674.
12 K. F. Hsu, S. Loo, F. Guo, W. Chen, J. S. Dyck, C. Uher, T. Hogan, E. K. Polychroniadis and M. G. Kanatzidis, *Science*, 2004, **303**, 818–821.
13 A. I. Boukai, Y. Bunimovich, J. Tahir-Kheli, J.-K. Yu, W. A. Goddard, III and J. R. Heath, *Nature*, 2008, **451**, 168–171.
14 A. I. Hochbaum, R. Chen, R. D. Delgado, W. Liang, E. C. Garnett, M. Najarian, A. Majumdar and P. Yang, *Nature*, 2008, **451**, 163–167.
15 G. H. Zhu, H. Lee, Y. C. Lan, X. W. Wang, G. Joshi, D. Z. Wang, J. Yang, D. Vashaee, H. Guilbert, A. Pillitteri, M. S. Dresselhaus, G. Chen and Z. F. Ren, *Phys. Rev. Lett.*, 2009, **102**, 196803/1–196803/4.
16 J. He, A. Gueguen, J. R. Sootsman, J.-C. Zheng, L. Wu, Y. Zhu, M. G. Kanatzidis and V. P. Dravid, *J. Am. Chem. Soc.*, 2009, **131**, 17828–17835.
17 L. D. Hicks, T. C. Harman and T. C. Dresselhaus, *Appl. Phys. Lett.*, 1993, **63**, 3230–3232.
18 L. D. Hicks and M. S. Dresselhaus, *Phys. Rev. B: Condens. Matter*, 1993, **47**, 12727–12731.

19 L. D. Hicks and M. S. Dresselhaus, *Phys. Rev. B: Condens. Matter*, 1993, **47**, 16631–16634.
20 M. S. Dresselhaus, Y. M. Lin, S. B. Cronin, M. R. Black, O. Rabin and G. Dresselhaus, *Therm. Conduct.*, 2005, **26**, 3–15; M. S. Dresselhaus, G. Chen, M. Y. Tang, R. Yang, H. Lee, D. Wang, Z. Ren, J.-P. Fleurial and P. Gogna, *Adv. Mater.*, 2007, **19**, 1043–1053.
21 S. K. Bux, J.-P. Fleurial and R. B. Kaner, *Chem. Commun.*, 2010, **46**, 8311–8324.
22 J. P. Heremans, *Springer Handbook of Nanotechnology* (2nd Ed.), 2007, 345–373; A. J. Minnich, M. S. Dresselhaus, Z. F. Ren and G. Chen, *Energy Environ. Sci.*, 2009, **2**, 466–479; Y. Lan, A. J. Minnich, G. Chen and Z. Ren, *Adv. Funct. Mater.*, 2010, **20**, 357–376; S. J. Thiagarajan, W. Wang and R. Yang, *Annu. Rev. Nano Res.*, 2010, **3**, 441–486.
23 J. R. Sootsman, D. Y. Chung and M. G. Kanatzidis, *Angew. Chem., Int. Ed.*, 2009, **48**, 8616–8639.
24 M. G. Kanatzidis, *Chem. Mater.*, 2010, **22**, 648–659.
25 E. S. Toberer, A. F. May and G. J. Snyder, *Chem. Mater.*, 2010, **22**, 624–634.
26 C. H. Champness, P. T. Chiang, K. Grabowski and W. B. Muir, *J. Appl. Phys.*, 1968, **39**, 4177–4183; K. S. V. L. Narasimhan, *Indian J. Pure Appl. Phys.*, 1967, **5**, 261–265.
27 D. M. Rowe, *CRC Handbook of Thermoelectrics*, CRC Press, Boca Raton, FL, 1994.
28 P. Carruthers, *Rev. Mod. Phys.*, 1961, **33**, 92–138.
29 M. S. Dresselhaus, G. Chen, Z. F. Ren, G. Dresselhaus, A. Henry and J. P. Fleurial, *J. Miner. Met. Mater. Soc.*, 2009, **61**, 86–90.
30 G. A. Slack, in *CRC Handbook of Thermoelectrics*, ed. D. M. Rowe, CRC Press, Boca Raton, FL, 1995, pp. 407–440.
31 G. A. Slack and M. A. Hussain, *J. Appl. Phys.*, 1991, **70**, 2694–718.
32 J. P. Dismukes, L. Ekstrom, E. F. Steigmeier, I. Kudman and D. S. Beers, *J. Appl. Phys.*, 1964, **35**, 2899–2907.
33 O. Beckman and P. Bergvall, *Ark. Fys.*, 1963, **24**, 113–22.
34 W. Zhao, P. Wei, Q. Zhang, C. Dong, L. Liu and X. Tang, *J. Am. Chem. Soc.*, 2009, **131**, 3713–3720.
35 A. Saramat, G. Svensson, A. E. C. Palmqvist, C. Stiewe, E. Mueller, D. Platzek, S. G. K. Williams, D. M. Rowe, J. D. Bryan and G. D. Stucky, *J. Appl. Phys.*, 2006, **99**, 023708/1–023708/5.
36 S. R. Brown, S. M. Kauzlarich, F. Gascoin and G. J. Snyder, *Chem. Mater.*, 2006, **18**, 1873–1877.
37 E. S. Toberer, C. A. Cox, S. R. Brown, T. Ikeda, A. F. May, S. M. Kauzlarich and G. J. Snyder, *Adv. Funct. Mater.*, 2008, **18**, 2795–2800.
38 V. K. Zaitsev, in *CRC Handbook Thermoelectrics*, ed. D. M. Rowe, CRC Press, Boca Raton, FL, 1995, pp. 299–309.
39 J. M. Higgins, A. L. Schmitt, I. A. Guzei and S. Jin, *J. Am. Chem. Soc.*, 2008, **130**, 16086–16094.
40 I. Aoyama, M. I. Fedorov, V. K. Zaitsev, F. Y. Solomkin, I. S. Eremin, A. Y. Samunin, M. Mukoujima, S. Sano and T. Tsuji, *Jpn. J. Appl. Phys.*, 2005, **44**, 8562–8570.
41 C. Vining, in *CRC Handbook of Thermoelectrics*, ed. D. M. Rowe, CRC Press, Boca Raton, FL, 1995, pp. 277–285.
42 J. P. Heremans, V. Jovovic, E. S. Toberer, A. Saramat, K. Kurosaki, A. Charoenphakdee, S. Yamanaka and G. J. Snyder, *Science*, 2008, **321**, 554–557.
43 G. D. Mahan, in *Solid State Physics: Advances in Research and Applications*, ed. H. Ehrenreich and F. Spaepen, Academic Press, San Diego, CA, 1998, pp. 81–157.
44 A. Boukai, K. Xu and J. R. Heath, *Adv. Mater.*, 2006, **18**, 864–869.
45 J. P. Heremans, C. M. Thrush, D. T. Morelli and M.-C. Wu, *Phys. Rev. Lett.*, 2003, **91**, 076804/1–076804/4.
46 S. K. Bux, R. G. Blair, P. K. Gogna, H. Lee, G. Chen, M. S. Dresselhaus, R. B. Kaner and J.-P. Fleurial, *Adv. Funct. Mater.*, 2009, **19**, 2445–2452.
47 N. F. Mott and H. Jones, *The Theory of the Properties of Metals and Alloys*, Dover Publications, New York, 1958.
48 A. S. Henry and G. Chen, *Journal of Computational and Theoretical Nanoscience*, 2008, **5**, 141–152.
49 G. A. Slack, *Solid State Phys.*, 1979, **34**, 1–71.
50 A. M. Morales and C. M. Lieber, *Science*, 1998, **279**, 208–211; Y. Xia, P. Yang, Y. Sun, Y. Wu, B. Mayers, B. Gates, Y. Yin, F. Kim and H. Yan, *Adv. Mater.*, 2003, **15**, 353–389.
51 J. L. Lensch-Falk, E. R. Hemesath, D. E. Perea and L. J. Lauhon, *J. Mater. Chem.*, 2009, **19**, 849–857.
52 M. J. Bierman, Y. K. A. Lau, A. V. Kvit, A. L. Schmitt and S. Jin, *Science*, 2008, **320**, 1060–1063; Y. K. A. Lau, D. J. Chernak, M. J. Bierman and S. Jin, *J. Am. Chem. Soc.*, 2009, **131**, 16461–16471; S. A. Morin, M. J. Bierman, J. Tong and S. Jin, *Science*, 2010, **328**, 476–480; S. Jin, M. J. Bierman and S. A. Morin, *J. Phys. Chem. Lett.*, 2010, **1**, 1472–1480.
53 Z. Zhang, J. Y. Ying and M. S. Dresselhaus, *J. Mater. Res.*, 1998, **13**, 1745–1748; K. G. Biswas, H. El Matbouly, V. Rawat, J. L. Schroeder and T. D. Sands, *Appl. Phys. Lett.*, 2009, **95**, 073108/1–073108/3.
54 J. Park, J. Joo, S. Kwon, Y. Jang and T. Hyeon, *Angew. Chem., Int. Ed.*, 2007, **46**, 4630–4660; Y. Yin and A. P. Alivisatos, *Nature*, 2005, **437**, 664–670.
55 I. A. Nishida, in *CRC Handbook of Thermoelectrics*, ed. D. M. Rowe, CRC Press, Boca Raton, FL, 1995, pp. 157–164.
56 S. B. Cronin, Y.-M. Lin, O. Rabin, M. R. Black, J. Y. Ying, M. S. Dresselhaus, P. L. Gai, J.-P. Minet and J.-P. Issi, *Nanotechnology*, 2002, **13**, 653–658.
57 R. Taylor, in *CRC Handbook of Thermoelectrics*, ed. D. M. Rowe, CRC Press, Boca Raton, FL, 1995, pp. 165–180.
58 D. G. Cahill, *Rev. Sci. Instrum.*, 1990, **61**, 802–808.
59 A. Mavrokefalos, A. L. Moore, M. T. Pettes, L. Shi, W. Wang and X. Li, *J. Appl. Phys.*, 2009, **105**, 104318/1–104318/8.
60 A. L. Moore, M. T. Pettes, F. Zhou and L. Shi, *Journal of Applied Physics*, 2009, 106; J. H. Zhou, C. G. Jin, J. H. Seol, X. G. Li and L. Shi, *Appl. Phys. Lett.*, 2005, **87**, 133109.
61 F. Zhou, A. L. Moore, M. T. Pettes, Y. Lee, J. H. Seol, Q. L. Ye, L. Rabenberg and L. Shi, *J. Phys. D: Appl. Phys.*, 2010, **43**, 025406/1–025406/9.
62 F. Zhou, J. Szczech, M. T. Pettes, A. L. Moore, S. Jin and L. Shi, *Nano Lett.*, 2007, **7**, 1649–1654.
63 L. Shi, Q. Hao, C. H. Yu, N. Mingo, X. Y. Kong and Z. L. Wang, *Appl. Phys. Lett.*, 2004, **84**, 2638–2640; C. Yu, Q. Hao, S. Saha, L. Shi, X. Y. Kong and Z. L. Wang, *Appl. Phys. Lett.*, 2005, **86**, 063101.
64 M. T. Pettes and L. Shi, *Adv. Funct. Mater.*, 2009, **19**, 3918–3925; C. H. Yu, L. Shi, Z. Yao, D. Y. Li and A. Majumdar, *Nano Lett.*, 2005, **5**, 1842–1846.
65 L. Shi, D. Li, C. Yu, W. Jang, D. Kim, Z. Yao, P. Kim and A. Majumdar, *J. Heat Transfer*, 2003, **125**, 881–888.
66 W. W. Cai, A. L. Moore, Y. W. Zhu, X. S. Li, S. S. Chen, L. Shi and R. S. Ruoff, *Nano Lett.*, 2010, **10**, 1645–1651; J. H. Seol, I. Jo, A. L. Moore, L. Lindsay, Z. H. Aitken, M. T. Pettes, X. S. Li, Z. Yao, R. Huang, D. Broido, N. Mingo, R. S. Ruoff and L. Shi, *Science*, 2010, **328**, 213–216.
67 P. Kim, L. Shi, A. Majumdar and P. L. McEuen, *Phys. Rev. Lett.*, 2001, **87**, 215502/1–215502/4; A. Mavrokefalos, M. T. Pettes, F. Zhou and L. Shi, *Rev. Sci. Instrum.*, 2007, **78**, 034901/1–034901/6.
68 J. Heremans and C. M. Thrush, *Phys. Rev. B: Condens. Matter Mater. Phys.*, 1999, **59**, 12579–12583.
69 M. Murata, D. Nakamura, Y. Hasegawa, T. Komine, T. Taguchi, S. Nakamura, C. M. Jaworski, V. Jovovic and J. P. Heremans, *J. Appl. Phys.*, 2009, **105**, 113706/1–113706/9; Y. Hasegawa, M. Murata, D. Nakamura, T. Komine, T. Taguchi and S. Nakamura, *J. Electron. Mater.*, 2009, **38**, 944–949.
70 M. Murata, D. Nakamura, Y. Hasegawa, T. Komine, T. Taguchi, S. Nakamura, V. Jovovic and J. P. Heremans, *Appl. Phys. Lett.*, 2009, **94**, 192104/1–192104/3; Y. Hasegawa, M. Murata, D. Nakamura and T. Komine, *J. Appl. Phys.*, 2009, **106**, 063703/1–063703/7.
71 A. Balandin and K. L. Wang, *J. Appl. Phys.*, 1998, **84**, 6149–6153.
72 J. O. Sofo and G. D. Mahan, *Appl. Phys. Lett.*, 1994, **65**, 2690–2692.
73 R. Venkatasubramanian, E. Siivola, T. Colpitts and B. O'Quinn, *Nature*, 2001, **413**, 597–602.
74 E. I. Rogacheva, O. N. Nashchekina, T. V. Tavrina, M. Us, M. S. Dresselhaus, S. B. Cronin and O. Rabin, *Phys. E.*, 2003, **17**, 313–315.
75 R. Yang and G. Chen, *Mater. Integr.*, 2005, **18**, 31–36.
76 L. D. Hicks, T. C. Harman, X. Sun and M. S. Dresselhaus, *Phys. Rev. B: Condens. Matter*, 1996, **53**, R10493–R10496.
77 E. I. Rogacheva, O. N. Nashchekina, A. V. Meriuts, S. G. Lyubchenko, M. S. Dresselhaus and G. Dresselhaus, *Appl. Phys. Lett.*, 2005, **86**, 063103/1–063103/3.

78 E. I. Rogacheva, O. N. Nashchekina, Y. O. Vekhov, M. S. Dresselhaus and S. B. Cronin, *Thin Solid Films*, 2003, **423**, 115–118.
79 F. W. Wise, *Acc. Chem. Res.*, 2000, **33**, 773–780.
80 W. Kim and A. Majumdar, *J. Appl. Phys.*, 2006, **99**, 084306/1–084306/7.
81 Y.-M. Lin and M. S. Dresselhaus, *Phys. Rev. B: Condens. Matter Mater. Phys.*, 2003, **68**, 075304/1–075304/14.
82 E. I. Rogacheva, O. N. Nashchekina, S. N. Grigorov, M. A. Us, M. S. Dresselhaus and S. B. Cronin, *Nanotechnology*, 2003, **14**, 53–59.
83 R. Venkatasubramanian, *Phys. Rev. B: Condens. Matter Mater. Phys.*, 2000, **61**, 3091–3097.
84 I. Chowdhury, R. Prasher, K. Lofgreen, G. Chrysler, S. Narasimhan, R. Mahajan, D. Koester, R. Alley and R. Venkatasubramanian, *Nat. Nanotechnol.*, 2009, **4**, 235–238.
85 G. D. Mahan and H. B. Lyon, Jr., *J. Appl. Phys.*, 1994, **76**, 1899–1901.
86 A. Bulusu and D. G. Walker, *J. Appl. Phys.*, 2007, **102**, 073713/1–073713/6.
87 V. Sandomirsky, A. V. Butenko, R. Levin and Y. Schlesinger, *J. Appl. Phys.*, 2001, **90**, 2370–2379.
88 I. Bejenari, V. Kantser and A. A. Balandin, *Phys. Rev. B: Condens. Matter Mater. Phys.*, 2010, **81**, 075316/1–075316/14.
89 R. Kim, S. Datta and M. S. Lundstrom, *J. Appl. Phys.*, 2009, **105**, 034506/1–034506/6.
90 T. Markussen, A.-P. Jauho and M. Brandbyge, *Phys. Rev. B: Condens. Matter Mater. Phys.*, 2009, **79**, 035415/1–035415/7.
91 T. Markussen, A.-P. Jauho and M. Brandbyge, *Nano Lett.*, 2008, **8**, 3771–3775.
92 Y.-M. Lin, X. Sun and M. S. Dresselhaus, *Phys. Rev. B: Condens. Matter Mater. Phys.*, 2000, **62**, 4610–4623.
93 J. P. Heremans, C. M. Thrush, D. T. Morelli and M.-C. Wu, *Phys. Rev. Lett.*, 2002, **88**, 216801/1–216801/4.
94 A. I. Persson, Y. K. Koh, D. G. Cahill, L. Samuelson and H. Linke, *Nano Lett.*, 2009, **9**, 4484–4488.
95 A. Mavrokefalos, M. T. Pettes, S. Saha, F. Zhou and L. Shi, *2006 25th International Conference on Thermoelectrics*, 2006, **25**, 234–237.
96 F. Zhou, J. H. Seol, A. L. Moore, L. Shi, Q. L. Ye and R. Scheffler, *J. Phys.: Condens. Matter*, 2006, **18**, 9651–9657; J. H. Seol, A. L. Moore, S. K. Saha, F. Zhou, L. Shi, Q. L. Ye, R. Scheffler, N. Mingo and T. Yamada, *J. Appl. Phys.*, 2007, **101**, 023706/1–023706/6.
97 X. Yang, G. Wang, P. Slattery, J. Z. Zhang and Y. Li, *Cryst. Growth Des.*, 2010, **10**, 2479–2482.
98 X. B. Zhao, X. H. Ji, Y. H. Zhang, T. J. Zhu, J. P. Tu and X. B. Zhang, *Appl. Phys. Lett.*, 2005, **86**, 062111/1–062111/3.
99 G. Zhang, Q. Yu, W. Wang and X. Li, *Adv. Mater.*, 2010, **22**, 1959–1962.
100 H. R. Shanks, P. D. Maycock, P. H. Sidles and G. C. Danielson, *Phys. Rev.*, 1963, **130**, 1743–1748.
101 L. Weber and E. Gmelin, *Appl. Phys. A: Mater. Sci. Process.*, 1991, **A53**, 136–140.
102 J. R. Heath, *Acc. Chem. Res.*, 2008, **41**, 1609–1617.
103 A. L. Schmitt, J. M. Higgins, J. R. Szczech and S. Jin, *J. Mater. Chem.*, 2010, **20**, 223–230.
104 D. G. Cahill, W. K. Ford, K. E. Goodson, G. D. Mahan, A. Majumdar, H. J. Maris, R. Merlin and S. R. Phillpot, *J. Appl. Phys.*, 2003, **93**, 793–818.
105 P. G. Klemens, *Proc. Phys. Soc., London*, 1955, **68A**, 1113–1128.
106 K. Kishimoto, M. Tsukamoto and T. Koyanagi, *J. Appl. Phys.*, 2002, **92**, 5331–5339; J. P. Heremans, C. M. Thrush and D. T. Morelli, *Phys. Rev. B: Condens. Matter Mater. Phys.*, 2004, **70**, 115334/1–115334/5; J. Martin, L. Wang, L. Chen and G. S. Nolas, *Phys. Rev. B: Condens. Matter Mater. Phys.*, 2009, **79**, 115311/1–115311/5.
107 A. Popescu, L. M. Woods, J. Martin and G. S. Nolas, *Phys. Rev. B: Condens. Matter Mater. Phys.*, 2009, **79**, 205302/1–205302/7.
108 M.-S. Jeng, R. Yang, D. Song and G. Chen, *J. Heat Tran.*, 2008, **130**, 042410/1–042410/11.
109 N. Mingo, D. Hauser, N. P. Kobayashi, M. Plissonnier and A. Shakouri, *Nano Lett.*, 2009, **9**, 711–715; Erratum in *Nano Lett.*, 2010, 10, p. 2288.
110 S. Wang and N. Mingo, *Appl. Phys. Lett.*, 2009, **94**, 203109/1–203109/3.
111 R. Yang, G. Chen and M. S. Dresselhaus, *Phys. Rev. B: Condens. Matter Mater. Phys.*, 2005, **72**, 125418/1–125418/7.
112 N. Mingo and D. A. Broido, *J. Appl. Phys.*, 2007, **101**, 014322/1–014322/7.
113 J. Martin, G. S. Nolas, W. Zhang and L. Chen, *Appl. Phys. Lett.*, 2007, **90**, 222112/1–222112/3.
114 X. Ke, C. Chen, J. Yang, L. Wu, J. Zhou, Q. Li, Y. Zhu and P. R. C. Kent, *Phys. Rev. Lett.*, 2009, **103**, 145502/1–145502/4.
115 W. Kim, J. Zide, A. Gossard, D. Klenov, S. Stemmer, A. Shakouri and A. Majumdar, *Phys. Rev. Lett.*, 2006, **96**, 045901/1–045901/4.
116 S. V. Faleev and F. Leonard, *Phys. Rev. B: Condens. Matter Mater. Phys.*, 2008, **77**, 214304/1–214304/9.
117 Y. Lan, B. Poudel, Y. Ma, D. Wang, M. S. Dresselhaus, G. Chen and Z. Ren, *Nano Lett.*, 2009, **9**, 1419–1422.
118 J. R. Sootsman, J. He, V. P. Dravid, C.-P. Li, C. Uher and M. G. Kanatzidis, *J. Appl. Phys.*, 2009, **105**, 083718/1–083718/8.
119 J. R. Sootsman, J. He, V. P. Dravid, S. Ballikaya, D. Vermeulen, C. Uher and M. G. Kanatzidis, *Chem. Mater.*, 2010, **22**, 869–875.
120 T. J. Zhu, F. Yan, X. B. Zhao, S. N. Zhang, Y. Chen and S. H. Yang, *J. Phys. D: Appl. Phys.*, 2007, **40**, 6094–6097.
121 W. Xie, X. Tang, Y. Yan, Q. Zhang and T. M. Tritt, *J. Appl. Phys.*, 2009, **105**, 113713/1–113713/8; W. Xie, X. Tang, Y. Yan, Q. Zhang and T. M. Tritt, *Appl. Phys. Lett.*, 2009, **94**, 102111/1–102111/3.
122 X. A. Fan, J. Y. Yang, Z. Xie, K. Li, W. Zhu, X. K. Duan, C. J. Xiao and Q. Q. Zhang, *J. Phys. D: Appl. Phys.*, 2007, **40**, 5975–5979.
123 X. B. Zhao, S. H. Yang, Y. Q. Cao, J. L. Mi, Q. Zhang and T. J. Zhu, *J. Electron. Mater.*, 2009, **38**, 1017–1024.
124 Y. Q. Cao, X. B. Zhao, T. J. Zhu, X. B. Zhang and J. P. Tu, *Appl. Phys. Lett.*, 2008, **92**, 143106/1–143106/3.
125 D. G. Ebling, A. Jacquot, H. Boettner, L. Kirste, J. Schmidt and M. Aguirre, *J. Electron. Mater.*, 2009, **38**, 1450–1455.
126 T. C. Harman, P. J. Taylor, M. P. Walsh and B. E. LaForge, *Science*, 2002, **297**, 2229–2232.
127 T. C. Harman, M. P. Walsh, B. E. Laforge and G. W. Turner, *J. Electron. Mater.*, 2005, **34**, L19–L22.
128 K. Ahn, M.-K. Han, J. He, J. Androulakis, S. Ballikaya, C. Uher, V. P. Dravid and M. G. Kanatzidis, *J. Am. Chem. Soc.*, 2010, **132**, 5227–5235.
129 J. R. Sootsman, H. Kong, C. Uher, J. J. D'Angelo, C.-I. Wu, T. P. Hogan, T. Caillat and M. G. Kanatzidis, *Angew. Chem., Int. Ed.*, 2008, **47**, 8618–8622.
130 T. Irie, *Jpn. J. Appl. Phys.*, 1966, **5**, 854–9.
131 E. Quarez, K.-F. Hsu, R. Pcionek, N. Frangis, E. K. Polychroniadis and M. G. Kanatzidis, *J. Am. Chem. Soc.*, 2005, **127**, 9177–9190; E. M. Levin, B. A. Cook, K. Ahn, M. G. Kanatzidis and K. Schmidt-Rohr, *Phys. Rev. B: Condens. Matter Mater. Phys.*, 2009, **80**, 115211/1–115211/6; L. Wu, J.-C. Zheng, J. Zhou, Q. Li, J. Yang and Y. Zhu, *J. Appl. Phys.*, 2009, **105**, 094317/1–094317/8; M. Zhou, J.-F. Li and T. Kita, *J. Am. Chem. Soc.*, 2008, **130**, 4527–4532.
132 X. Xin, Y. Jiang, D. Kong, H. Zhong, L. Chen and D. Yu, *Phys. Status Solidi A*, 2010, **207**, 163–169.
133 S. H. Yang, T. J. Zhu, T. Sun, J. He, S. N. Zhang and X. B. Zhao, *Nanotechnology*, 2008, **19**, 245707/1–245707/5; P. F. P. Poudeu, A. Gueguen, C.-I. Wu, T. Hogan and M. G. Kanatzidis, *Chem. Mater.*, 2010, **22**, 1046–1053.
134 C. B. Vining, W. Laskow, J. O. Hanson, R. R. Van der Beck and P. D. Gorsuch, *J. Appl. Phys.*, 1991, **69**, 4333–4340.
135 V. E. Borisenko, *Semiconducting Silicides*, Springer, Berlin, 2000.
136 V. K. Zaitsev, M. I. Fedorov, E. A. Gurieva, I. S. Eremin, P. P. Konstantinov, A. Y. Samunin and M. V. Vedernikov, *Phys. Rev. B: Condens. Matter Mater. Phys.*, 2006, **74**, 045207/1–045207/5.
137 I. Aoyama, H. Kaibe, L. Rauscher, T. Kanda, M. Mukoujima, S. Sano and T. Tsuji, *Jpn. J. Appl. Phys.*, 2005, **44**, 4275–4281.
138 T. Dasgupta, J. Etourneau, B. Chevalier, S. F. Matar and A. M. Umarji, *J. Appl. Phys.*, 2008, **103**, 113516/1–113516/7; I. Nishida, *J. Mater. Sci.*, 1972, **7**, 1119.
139 U. Birkholz, E. Groβ and U. Stohrer, in *CRC Handbook of Thermoelectrics*, ed. D. M. Rowe, CRC Press, Boca Raton, FL, 1995, pp. 287–299.
140 M. Ito, T. Tanaka and S. Hara, *J. Appl. Phys.*, 2004, **95**, 6209–6215.
141 M. I. Fedorov, *J. Thermoelectr.*, 2009, 51–60.

142 Q. Zhang, J. He, T. J. Zhu, S. N. Zhang, X. B. Zhao and T. M. Tritt, *Appl. Phys. Lett.*, 2008, **93**, 102109/1–102109/3.
143 M. Yang, W. Luo, Q. Shen, H. Jiang and L. Zhang, *Adv. Mater. Res.*, 2009, **66**, 17–20.
144 J. R. Szczech and S. Jin, *J. Solid State Chem.*, 2008, **181**, 1565–1570.
145 A. J. Zhou, X. B. Zhao, T. J. Zhu, Y. Q. Cao, C. Stiewe, R. Hassdorf and E. Mueller, *J. Electron. Mater.*, 2009, **38**, 1072–1077.
146 J. Schumann, C. Gladun, J. I. Moench, A. Heinrich, J. Thomas and W. Pitschke, *Thin Solid Films*, 1994, **246**, 24–29.
147 N. Scoville, C. Bajgar, J. Rolfe, J. P. Fleurial and J. Vandersande, *Nanostruct. Mater.*, 1995, **5**, 207–223.
148 F. Brochin, B. Lenoir, X. Devaux, R. Martin-Lopez and H. Scherrer, *J. Appl. Phys.*, 2000, **88**, 3269–3275.
149 N. Gothard, X. Ji, J. He and T. M. Tritt, *J. Appl. Phys.*, 2008, **103**, 054314/1–054314/4.